UNIVERSIDADE FEDERAL DO PARANÁ

ISADORA FERREIRA CAIXETA

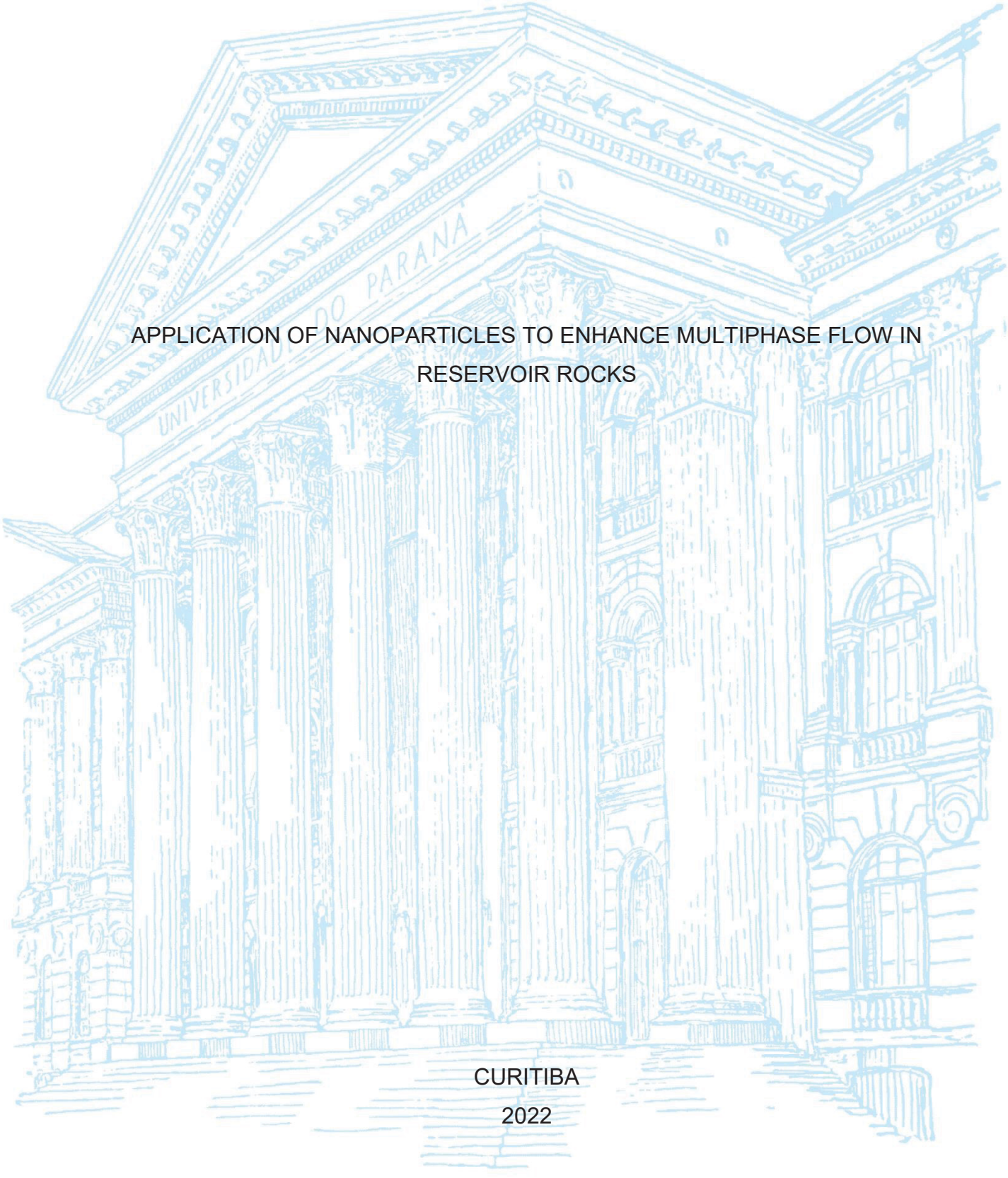


# APPLICATION OF NANOPARTICLES TO ENHANCE MULTIPHASE FLOW IN RESERVOIR ROCKS

CURITIBA

2022

ISADORA FERREIRA CAIXETA

# APPLICATION OF NANOPARTICLES TO ENHANCE MULTIPHASE FLOW IN RESERVOIR ROCKS

Dissertação apresentada ao Programa de Pós-Graduação em Engenharia Química – PPGEQ, Setor de Tecnologia, Universidade Federal do Paraná como requisito parcial para obtenção do título de Mestre em Engenharia Química.

Orientador: Prof. Dr. Luiz Fernando de Lima Luz Junior.

Coorientadores: Profª. Dra. Anelize Manuela Bahniuk Rumbelsperger e Dra. Nathaly Lopes Archilha.

CURITIBA

2022

DADOS INTERNACIONAIS DE CATALOGAÇÃO NA PUBLICAÇÃO (CIP)
UNIVERSIDADE FEDERAL DO PARANÁ
SISTEMA DE BIBLIOTECAS – BIBLIOTECA CIÊNCIA E TECNOLOGIA

Caixeta, Isadora Ferreira.
Application of nanoparticles to enhance multiphase flow in reservoir rocks. / Isadora Ferreira Caixeta. – Curitiba, 2023.
1 recurso on-line : PDF.

Dissertação (Mestrado) – Universidade Federal do Paraná, Setor de Tecnologia, Programa de Pós-Graduação em Engenharia Química.
Orientador: Prof. Dr. Luiz Fernando de Lima Luz Junior.
Cooriendadora: Profa. Dra. Anelize Manuela Bahniuk Rumbelsperger.
Cooriendadora: Profa. Dra. Nathaly Lopes Archilha.

1. Engenharia do petróleo. 2. Nanotecnologia. 3. Raio X – Aplicações industriais. 4. Rochas carbonáticas. I. Luz Junior, Luiz Fernando de Lima. II. Rumbelsperger, Anelize Manuela Bahniuk. III. Archilha, Nathaly Lopes. IV. Universidade Federal do Paraná. Programa de Pós-Graduação em Engenharia Química. V. Título.

Bibliotecário: Nilson Carlos Vieira Júnior CRB-9/1797

# TERMO DE APROVAÇÃO

Os membros da Banca Examinadora designada pelo Colegiado do Programa de Pós-Graduação ENGENHARIA QUÍMICA da Universidade Federal do Paraná foram convocados para realizar a arguição da dissertação de Mestrado de **ISADORA FERREIRA CAIXETA** intitulada: **APPLICATION OF NANOPARTICLES TO ENHANCE MULTIPHASE FLOW IN RESERVOIR ROCKS**, sob orientação do Prof. Dr. LUIZ FERNANDO DE LIMA LUZ JUNIOR, que após terem inquirido a aluna e realizada a avaliação do trabalho, são de parecer pela sua APROVAÇÃO no rito de defesa.

A outorga do título de mestra está sujeita à homologação pelo colegiado, ao atendimento de todas as indicações e correções solicitadas pela banca e ao pleno atendimento das demandas regimentais do Programa de Pós-Graduação.

CURITIBA, 14 de Outubro de 2022.

Assinatura Eletrônica
14/10/2022 11:27:26.0
LUIZ FERNANDO DE LIMA LUZ JUNIOR
Presidente da Banca Examinadora

Assinatura Eletrônica
14/10/2022 12:29:46.0
MARCELO KAMINSKI LENZI
Avaliador Interno (UNIVERSIDADE FEDERAL DO PARANÁ)

Assinatura Eletrônica
14/10/2022 11:10:50.0
REGINA WEINSCHUTZ
Avaliador Externo (UNIVERSIDADE FEDERAL DO PARANÁ )

## RESUMO

A depleção natural e a diminuição da taxa de recuperação nas instalações de extração de hidrocarbonetos acarretam na utilização de técnicas avançadas de recuperação, em inglês Enhanced Oil Recovery (EOR), para o aumento do fator de recuperação do reservatório. Neste estudo foi avaliada a ação de nanopartículas de sílica (SiN) em solução, na etapa EOR, utilizando a microtomografia de raio X (μCT) para avaliar o arranjo de óleo/fase aquosa, na escala de poro. As NP de 30, 60 e 100 nm de diâmetro foram sintetizadas pelo método de Stöber modificado e caracterizadas por análises de Dynamic light scattering (DLS), potencial zeta, Scanning Electron Microscopy (SEM). Com a análise das imagens obtidas na μCT foi observado que as SiN-30 e SiN-60 tiveram pouco efeito quando comparadas com a SIN-100, a qual apresentou uma ação substancial na mobilização e na remoção de óleo mesmo em baixas concentrações, aumentando a recuperação de 44 para 56% do volume inicial de óleo. Experiências adicionais aumentando a concentração de SiN-100 nm mostraram que para este sistema, a nanopartícula de sílica óptima permanece a uma baixa concentração de 0,05 wt%.



**Palavras-chave:** Microtomografia de raios X, nanopartículas de sílica, recuperação avançada de petróleo, nanotecnologia, engenharia de reservatório, rochas carbonáticas.

## ABSTRACT

The natural depletion and the reduction of the recovery rate in the hydrocarbon extraction facilities lead to the use of advanced recovery techniques, known as Enhanced Oil Recovery (EOR), to increase the reservoir Recovery Factor. In this study, the action of silica nanoparticles (SiN) solution was evaluated in the EOR phase, using X-ray microtomography (μCT) to evaluate the oil/aqueous phases arrangement in the pore scale. The SiN of 30, 60, and 100 nm in diameter were synthesized by the modified Stöber method and characterized by Dynamic light scattering (DLS), Zeta potential, and Scanning Electron Microscopy (SEM). From the image analysis obtained from the μCT images, it was observed that the SiN -30 and SiN -60 had a slight effect on the oil recovery in comparison to SiN -100 which presented a substantial action in the mobilization and removal of oil, even at low concentrations, increasing the recovery from 44 to 56% of the initial volume of oil. Additional experiments increasing the concentration of SiN-100 nm showed that for this system, the optimal silica nanoparticle remains at a low concentration of 0.05 wt%.



**Keywords:** X-ray tomography, silica nanoparticles, enhanced oil recovery, nanotechnology, reservoir engineering, carbonate rocks.

## FIGURES LIST

## TABLES LIST

## ABREVIATIONS LIST

AAPG – American Association of Petroleum Geologists.

ANP – Agência Nacional de Petróleo Gás Natural e Biocombustíveis

BPR – Backpressure regulator

CNPEM – Centro Nacional de Pesquisa em Energia e Materiais

CT – Computed tomography

COBR – Crude oil-brine-rock

DLS – Dynamic light scattering

EOR – *Enhanced Oil Recovery*

FCO – Foreign and Commonwealth Office

FBP – Filtered back projection

FTIR – Fourier-transform Infrared spectroscopy

IEA – International Energy Agency

IFT – Interfacial tenson

IMX – Linha de Luz de Microtomografia por Raios-X

LAMIR – Instituto Laboratório de Análise de Minerais e Rochas

NP – Nanoparticle

SEM – Scanning Electron Microscopy

SiN – Silica nanoparticle

TEOS – Tetraethyl orthosilicate

UK – United Kingdom

ZP – Zeta potential

μCT – X-ray microtomography

%wt – Weight percentage

## SYMBOLS LIST

| | | |
|---|---|---|
| A | Cross-section area of flow | [m²] |
| k | Average rock permeability | μm²] |
| K | Absolute permeability | [μm²] |
| $k_{ro}$ | Oil relative permeability | [dimensionless] |
| $k_{rw}$ | Water relative permeability | [dimensionless] |
| L | length | [m] |
| Nc | Capillary number | [dimensionless] |
| $S_g$ | Gas saturation | [fraction] |
| $S_l$ | Saturation of phase “l” | [fraction] |
| $S_o$ | Oil saturation | [fraction] |
| $S_w$ | Water saturation | [fraction] |
| $S_{wc}$ | Connate water or irreducible water saturation | [fraction] |
| $S^*$ | Normalized wetting phase saturation | [fraction] |
| q | Volumetric flow rate | [$m^3/s$] |
| $q_o$ | Darcy velocity of oil phase | [m/s] |
| $q_w$ | Darcy velocity of water phase | [m/s] |
| v | Fluid velocity | [m/s] |
| V | Linear velocity | [m/s] |
| $V_l$ | Phase volume | [m³] |
| $V_p$ | Pore volume | [m³] |
| °API | American Petroleum Institute gravity | [dimensionless] |
| μ | Viscosity of the displacing fluid phase | [Pa.s] |
| $\mu_o$ | Viscosity of oil | [Pa.s] |
| $\mu_w$ | Viscosity of water | [Pa.s] |
| σ | Interfacial tension | [N/m] |
| γ | Specific gravity | [dimensionless] |
| $\rho_o$ | Oil or any mixture density | [kg/m³] |
| $\rho_w$ | Water density | [kg/m³] |
| θ | Angle | [Degrees] |
| Δp | Pressure diferential | [Pa] |
| δp/δL | Pressure gradient that drives the fluid | [Pa/m] |

## TABLE OF CONTENTS

# 1 INTRODUCTION

In a worldly scenario, more than 98 Mb/d (millions of barrels per day) of oil was consumed in 2019, of which Brazil was responsible for 3.1%, moreover, in this same year, the overall annual demand for oil increased by 0.92 Mb/d (BRITISH PETROLEUM, 2020). According to the Brazilian Petroleum, Natural Gas and Biofuels Agency (Agência Nacional de Petróleo Gás Natural e Biocombustíveis – ANP) (2020), in 2019, the pre-salt reservoirs explorations had an important and the main share in oil production, nationally the average was 2.8Mb/d of petroleum. Even with this production rate country depends on petroleum importation to supply consuming inner demand.

Currently, available petroleum reserves can supply 50 years maximum, for global production, based on the 2019 annual reserves-to-production rate (BRITISH PETROLEUM, 2020). Besides, the exploration/production units are reaching their maturity stage in several countries, and new reservoir areas are rarely discovered, leading to production decay, so there is a development need for new technologies and recovery methods (CHANDLER, 2017).

Petroleum industries require essential information to monitor their production, such as the recovery faction, production rate, petroleum amount available in reservoirs to be recovered, etc. In reference to recovery factor property, it determines reservoir production limits in each of the classic recovery stages, primary production, secondary, and tertiary or Enhanced Oil Recovery (EOR) (SMALLEY *et al*., 2009). In the first recovery, less than 20% of the available oil is recovered, thus the secondary (waterflooding) and tertiary are implemented to increase this percentual through fluids injection (*e.g*. water, CO2, surfactants, nanoparticles), ensuring the well maintenance and the petroleum supplying demands (PAK *et al*., 2018).

Oil volumes accumulate in micro and nanometric porous spaces that constitute the reservoir rocks (*e.g*. carbonates, sandstones, dolomites). Hence, nanoparticles, like silica-based ones, beyond their capability to change reservoir dynamics properties (viscosity, wettability, etc.), also have certain displacement efficiency inside the porous media. Recent studies demonstrate the nanoparticle mechanisms of action in rock samples, showing their effects and applicability in the EOR process process (HENDRANINGRAT; LI; TORSATER, 2013, PAK *et al*., 2018).

## 1.1 OBJECTIVES

### 1.1.1 Main objective

Evaluate the size and concentration of silica nanoparticles in oil/gas/aqueous phase arrangement in different porous medium, making observations in porous scale, aiming an enhanced oil recovery through nanoflooding.

### 1.1.2 Specific objectives

- Perform flow experiments using a mimic porous medium, with glass beads and ooids;
- Analyze through tridimensional images obtained by X-ray microtomography the oil retention, degradation and remobilization;
- Study the interaction between the nanoparticles and the other phases;
- Find the injection efficiency of nanoparticles solution, as a EOR technology.

# 2 LITERATURE REVIEW

## 2.1 RESERVOIRS

Hydrocarbons, oil, or gases, are generated at subsurface depths under particular conditions and combinations of specific factors such as temperature, pressure, organic matter, and sediment quantities (THOMAS, 2001). Hydrocarbon generations occur in a different rock than the one they accumulate, therefor the oil formed needs to be expelled from the source rock to the reservoir, FIGURE 2.1 shows this mechanism of oil migration.

FIGURE 2.1 – Oil production rate in recovery process stages

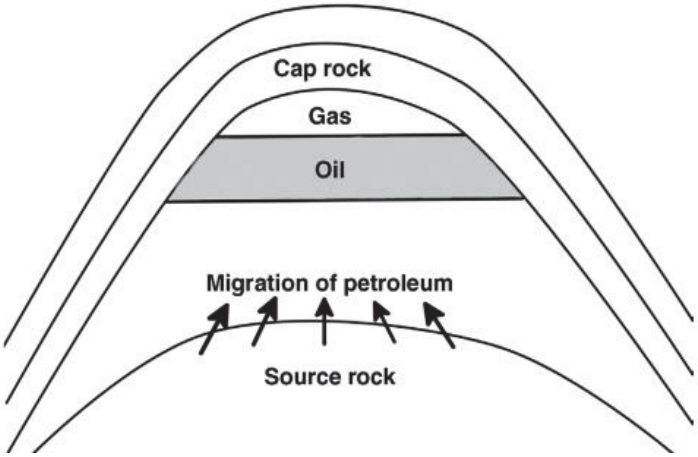


SOURCE: SATTER; IQBAL (2016)

Source rocks are fine-grained sedimentary rocks composed mainly of fine-grained shale and mudstone, enriched in clay, and some carbonate source rocks are also reported. According to ULMISHEK AND KLEMME (1990), source rocks from six stratigraphic intervals in Phanerozoic time (Silurian, Upper Devonian-Tournaisian, Pennsylvanian-Lower Permian, Upper Jurassic, middle Cretaceous, and Oligocene-Miocene) contain more than 90% of the world original oil reserves. These rocks have less porosity due to compaction, which is why the first phase of the two-step oil migration mechanism is an open discussion to the scientific community. Regarding secondary migration, geological studies indicate that this step begins after the oil reaches the boundaries of the reservoir rock, which water previously occupied the rock pores, and then by displacing from it through gravity and capillary pressure. The

existence of microfractures, flaws, pore channels, and joints contribute to oil migration (SATTER; IQBAL, 2016; SPEIGHT, 2020).

To stop the oil flow and allow it to accumulate in the reservoir, are trapping mechanisms and geologic features after these rocks, which have a classification as structural, stratigraphic, or a combination of both (THOMAS, 2001). These containment traps sometimes are covered by sealing rocks with low permeability that stops the flow (SATTER; IQBAL, 2016).

The oil generation, migration, accumulation, trapping processes, and the types of rocks related to, described in this system, only take into account in conventional reservoirs. In unconventional reservoirs, for example, crude oil is not trapped by seal rock or cap rock, typically it has low or ultralow permeability, so the oil flow is significantly lower, and often the source and reservoir rocks are the same (SATTER; IQBAL, 2016; SPEIGHT, 2020).

Carbonate rocks are the third most common type of sedimentary rock found in reservoir fields, with sandstone being the most abundant (SPEIGHT, 2020). To classify carbonate rocks is necessary to identify their basics components, type of grain (solid particles in the sediment), matrix (finest material deposited between the grains), and cementitious character (way in which certain minerals bind the rock's grains) (TERRA *et al*., 2010; SATTER; IQBAL, 2016). The classic sedimentary/carbonate rocks classifications are those proposed by Folk (FIGURE 2.2) and Dunham (FIGURE 2.3).

FIGURE 2.2 – Carbonate rock graphic classification table proposed by Folk

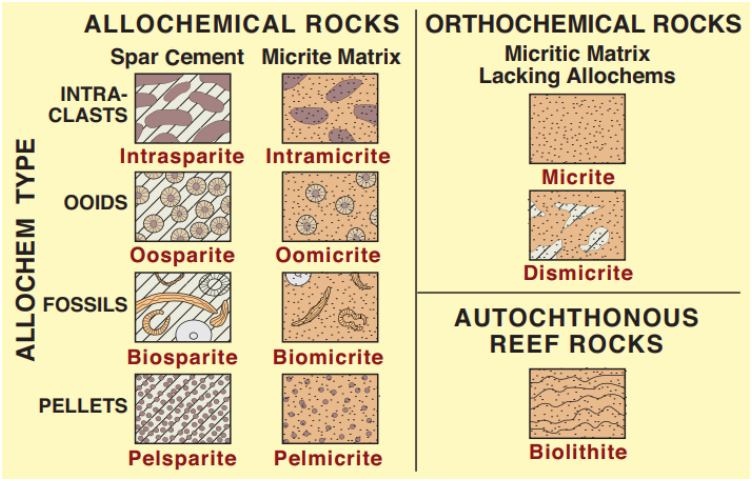


SOURCE: AAPG (2003).

FIGURE 2.3 – Classification table of carbonate rocks according with Dunham

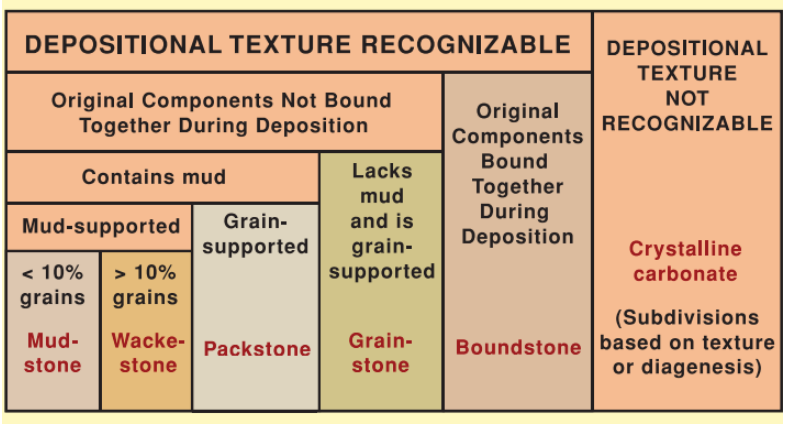


SOURCE: AAPG (2003)

Folk classification (FIGURE 2.2 is composition based, where he proposed eleven basic terms whose basal names come from four-grain types. In the meantime, Dunham classification (FIGURE 2.3) relied on depositional texture, which formed its four-main names according to relative percentages of grain and mud (TERRA *et al*., 2010; AAPG, 2003).

## 2.2 ROCK AND FLUID PROPERTIES

The oil initially in place (OOIP) in a reservoir depends on rock and fluids properties; moreover, the amount of available oil to be recovered and the forward needing methods to do it are also significantly influenced by the reservoir's features.

### 2.2.1 Porosity

Porosity is related to reservoir storage capacity and consists of the micro and nano pores network volume, which generally ranges between 5 and 25%, depending on rock type (SATTER; IQBAL, 2016). This property is defined by: the volume of pore spaces divided by the bulk volume of the rock, where the bulk volume is the total of pores plus solid matrix volume in the rock (Equation 2.1).

$$\text{Porosity, \%} = \frac{\text{Pore spaces volume}}{\text{Total volume of rock}} \times 100 \qquad (2.1)$$

A real-world rock can be related to two types of porosity, absolute porosity, which includes the total pore volume, and effective porosity, which only considers interconnected pore spaces. Between these two, the core concern of the oil production segment is the effective porosity as these are the pores that can produce oil and gas, those that do not have a dead-end, allowing flow to occur (ERKETIN; ABOU-KASSEM; KING, 2001; SATTER; IQBAL, 2016).

In addition, sedimentary rocks are found at different depths, undergoing variations in internal pressure and changes in grains and pores by fluid flow, interfering with compaction and porous volume (ROSA; CARVALHO; XAVIER, 2006). Carbonates particularly have complex porosity with different pore geometries and size distribution; their abundant microporosity and presence of sub-micron structures make it challenging to characterize and evaluate porosity, impacting field performance understanding (GHOUS *et al*., 2007).

### 2.2.2 Fluid saturation

In a reservoir, each fluid phase has its saturation and is an unsettling property for petroleum engineering since it varies according to location and time inside it, affecting its production, especially when, for oil recovery, there is a fluid injection (SATTER; IQBAL, 2016).

The saturation for each fluid present in the reservoir represents the volume fraction occupied by them in the reservoir pores, as shown in Equation (2.2):

$$S_l = \frac{V_l}{V_p} \tag{2.2}$$

where $S_l$ and $V_l$ ($m^3$) are the saturation and the volume phase (oil “o”, water “w” and gas “g”), respectively, and $V_p$ ($m^3$) is the total pore volume of the reservoir (ERKETIN; ABOU-KASSEM; KING, 2001). Therefore, for a reservoir composed of oil, water, and gas, the saturations can be related to Equation (2.3).

$$S_o + S_w + S_g = 1 \tag{2.3}$$

### 2.2.3 Permeability

Permeability is a reservoir property that indicates how easily a fluid flows through porous media. The definition of permeability stated by the empirical correlation known as Darcy's Law is valid only for water, then beyond, to other fluids (*e.g*. gas, oil) was added to this equation the fluid viscosity effect. That modification is presented as shown in Equation (2.4).

$$v = \frac{q}{A} = -\left(\frac{k}{\mu}\right)\left(\frac{\delta p}{\delta L}\right) \tag{2.4}$$

where v is the fluid velocity; k is the average rock permeability; μ is the fluid viscosity and δp/δL the pressure gradient that drives the fluid.

Absolute permeability (permeability of the medium) equation, referred to above, is restricted to a steady-state laminar flow, to a homogeneous porous medium, and valid for a single-phase flow. It is a significant rock's feature for production rate, where the higher its property value, the better the well productivity (SATTER; IQBAL, 2016).

Since Darcy's law does not apply to two or more fluid phases, it can be changed to calculate relative permeability, which is related to the flow of each phase. The equations to calculate relative permeability are presented below (GAO *et al.*, 2020; ERKETIN; ABOU-KASSEM; KING, 2001).

$$k_{rw} = \frac{q_w \mu_w L}{\Delta p\, K} \tag{2.5}$$

$$k_{ro} = \frac{q_o \mu_o L}{\Delta p\, K} \tag{2.6}$$

where $k_r$ and q is the relative permeability and the Darcy's velocity of each phase (w – water phase, o – oil phase), successively, μ is the viscosity, L is the length of the whole sample, Δp is the pressure differential along the sample and K is the absolute permeability.

Relative permeability can be measured based on fluid saturations, this type of correlation is used in the lack of field data. The following equations are applied for oolitic limestone, cemented sandstone, and vugular rocks (SATTER; IQBAL, 2016):

Oil- water relative permeabilities:

$$k_{ro} = \left(1 - S^{*}\right)^{2}\left(1 - S^{*2}\right)$$
$$k_{rw} = \left(S^{*}\right)^{4} \quad (2.7)$$

Where the S* is calculated by the Equation (2.8), for oil-water system:

$$S^{*} = \frac{S_w - S_{wc}}{1 - S_{wc}} \quad (2.8)$$

$S_{wc}$ = connate water or irreducible water saturation.

Irreducible water saturation fraction occurs when the water becomes immobile, which is the lower value of initial water saturation.

### 2.2.4 Wettability

In oil recovery, wettability is a significant surface characteristic, which indicates the rock surface preference to be in contact with one fluid in the presence of another, having a strong influence on oil displacement microscopic efficiency and in the ultimate achievable recovery factor, due to its impact on relevant properties such as permeability and capillary pressure. This relation occurs because wettability controls the distribution of fluids in a porous medium, also their location and flow (DING; GAO, 2021; ANDERSON, 1987; SATTER; IQBAL, 2016).

Wettability is controlled by the crude oil-brine-rock (COBR) interactions. It is a scale-dependent property, which has been measured so far by adhesion forces (molecular scale), contact angle (sub and large pore scale), fluid distribution, local capillarity pressure, and small-scale relative permeability (pore network). The contact angle is one of the most accepted and used methods for wettability measurement in COBR systems. However, it is limited because it provides only average values, has

large-scale resolutions, and is subject to contact angle hysteresis (RUECKER, 2020). By this method, the system's wettability can be classified according to the contact angle of the water phase; if – $\theta > 90°$ water wet, $\theta < 90°$ is oil wet, and $\theta = 90°$ intermediate wettability (FORREST; CRAIG, 1971).

### 2.2.5 Specific gravity and API gravity

Specific gravity ($\gamma$) of oil or any mixture is defined as the ratio of its density ($\rho_o$) by the water density ($\rho_w$), both measured at the same condition of pressure and temperature, as presented in Equation (2.9):

$$\gamma = \frac{\rho_o}{\rho_w} \tag{2.9}$$

In the petroleum industry, specific gravity is commonly expressed in terms of API gravity (°API), as defined by the American Petroleum Institute is calculated at a standard temperature of 60° by the following equation:

$$°API = \frac{141,5}{\gamma} - 131,5 \tag{2.10}$$

where $\gamma$ is the specific gravity of the substance, dimensionless.

The °API is proportionally inverse to specific gravity, so to dense oils, this property has a low value, typically having the highest prices on the market. Because reservoir fluids (gas, oil, brine/water) have different specific gravity, their relative positions assist in determining the well drilling area, avoiding gas or water production, and maximizing oil production (SATTER; IQBAL, 2016).

### 2.2.6 Capillary Number

The recovery efficiency in oil reservoirs is influenced by three forces: gravity, viscous and capillary, considering when a fluid displaces another immiscible one. The gravity force is set by the density difference of fluids in the reservoir, while viscous forces outcome from fluid viscosities and the pressure gradient that acts on fluid

dynamics. Capillary forces, in contrast, result from interfacial tension of reservoir fluids, rock wettability, and pore structure (FORREST; CRAIG, 1971; CHATZIS; MORROW, 1984).

As displacement efficiency is related to the competition of these forces in the system, the capillary number, the dimensionless ratio of viscous to capillary forces, was found to be responsible for the entrapment and dynamics of fluids in a porous media. The capillary number can define the flow regimes and the recovery efficiency, and by a modification of Darcy's equation can be obtained the classic definition of this expression:

$$Nc = \frac{V \cdot \mu}{\sigma} \tag{2.11}$$

where V (m/s) is the linear velocity and μ (Pa.s) is viscosity of the displacing fluid phase and σ (N/m) is the interfacial tension between the two fluid phases. Many mathematical definitions and studies, of theory, after that, were proposed to represent the porous media heterogeneity, porosity, and permeability, to better correspond to fluid and displacement methods (GUO *et al.,* 2015; GARNES *et al.*, 1990).

## 2.3 OIL RECOVERY STAGES

Usually, in the oil industry, oil recovery occurs in three stages: primary, secondary, and tertiary (also called Enhanced Oil Recovery – EOR), where the main goal is to enhance hydrocarbon production. Primary recovery is a natural process that depends on the pressure gradient between the surface and internal energy (pore pressure) of the reservoir (SHENG, 2011); however, less than 20% of available oil is recovered at this stage (FCO, 2017).

Secondary recovery usually initiates a few years after the beginning of well exploration, when the natural depletion of energy starts and the production rate decay. This recovery stage is characterized by the external fluids injection, usually immiscible, into the reservoir to increase internal pressure and drive the oil up through the well. Commonly known as well by waterflooding, the most used fluid is water due to its availability and low cost (IEA, 2015).

Waterflooding is applied to maintain the dissolved gases in the solution when injected above the bubble point pressure. In addition, at the beginning of injection, the water helps preserve the reservoir pressure by filling up the pores occupied by free gases. These applications also contribute to production rate increases (SATTER; IQBAL, 2016), with a maximum recovery oil volume rate of 40% of the original oil in place, at this stage, hence a significant amount of oil or gas remaining inside the reservoir (FCO, 2017).

Enhance Oil Recovery (EOR), or tertiary recovery, implementation intention is to increase the recovery rate percentage when the conventional methods performed in the other stages are no longer effective. Utilizing other fluids (*e.g.*, $CO_2$, surfactants, nanoparticles) injections or thermal energy in the reservoir, at this stage, the production rate can extract 60% or more of the original oil available, and the percentage depends on the type of injection. Furthermore, the EOR method selection relies on the mineral composition of the rock and fluid present in the reservoir, which is unique for each reservoir (SHENG, 2011).

### 2.3.1 Gas injection

Recover oil by miscible displacement methods, in most cases, uses light to intermediate hydrocarbons or $CO_2$. The injection of hydrocarbons into reservoirs leads to the formation of a miscible flood front that causes the oil to rise. And to achieve this miscibility, the fields often use natural gas enriched with ethane or injected gas (*e.g.* methane at high pressure) that vaporizes light to the intermediate components of the oil (SATTER; IQBAL, 2016).

Adversely, hydrocarbon injection, in its application, employs expensive products on a large scale, which possibly cannot be recovered. A reservoir minimum depth application is another limitation of this process; for instance, the shallow reservoir does not possess the required pressure, so it cannot generate the miscible conditions needed. Additionally, it causes the formation of viscous fingering due to the viscosity difference with the oil injected, which these fluids can result in a poor sweep (SATTER; IQBAL, 2016).

Carbon dioxide flooding uses a significant amount of $CO_2$ at high pressure, using 95% v/v or higher purity, to reach miscibility conditions. Moreover, $CO_2$ reduces

capillary forces creating a more favorable flow property, such as a viscosity reduction, before achieving miscibility. Compared to other miscible displacement methods, $CO_2$ injection is suitable for a wide range of reservoirs due to its efficiency at lower miscibility pressure (2200-3200 psi, under conventional reservoir conditions). The limitations of this process include the difficulty of $CO_2$ separation from the product, possible corrosion in wells, and the necessity of $CO_2$ in large amounts (SATTER; IQBAL, 2016; IEA, 2015).

### 2.3.2 Chemical injection

Chemical injections consist of the addition of a chemical component such as polymer, micellar-polymer, surfactant, and alkaline materials to reservoir flooding to reduce the interfacial tension between the fluids and increase viscosity, or reduce the injected fluid mobility, thereby improving sweep efficiency (SATTER; IQBAL, 2016; VISHNYAKOV *et al.*, 2020).

In this EOR method, a broad selection of chemical products are applied (WANG; LIU; GU, 2003; ZHANG; LI; ZHOU, 2011; GUO *et al.*, 2011; HAN *et al.*, 2013; LEVITT *et al.*, 2006), including a combination of this method with others, known as the hybrid process; (ALSOFI; WANG; KAIDAR, 2018; WANG *et al.*, 2020; SHAKEEL *et al.*, 2021) furthermore, others are being developed and tested even now (RAMOS; AKANJI; AFZAL, 2020; KHAYATI, 2020; NAFISIFAR; MANSHAD; SHADIZADEH, 2021).

In polymer flooding, a water-soluble polymer is added to the injected water, usually at low concentrations. There are two main types of polymers applied in EOR: synthetic and biopolymer, an example of common polymer used by these two groups are the HPAM (hydrolyzed polyacrylamide) and Xanthan, as follow (SHENG, 2011; MOHSENATABAR; SAGHAFI, 2020).

The main mechanisms of polymers solubilization in the injected water are: increasing the viscosity and altering to a non-Newtonian fluid, conferring, this latter to the water, characteristics of a polymeric solution, such as shear thinning or pseudoplastic rheology. Moreover, water-soluble polymers are anionic surfactants, therefore, acting also by reducing the surface tension of the water (SATTER; IQBAL, 2016; VISHNYAKOV *et al.*, 2020).

Oil displacement is improved because these mechanisms ensure a more stable water-oil flood front, reducing the fingering process and retarding water breakthrough. Despite these advantages, polymer flooding has problems at the injection point, requiring higher pressures to be economically viable relative to water flooding. Besides, it has a higher probability of well clogging and usually needs more wells. Beyond that, depending on the polymer type, there is the potential for its adsorption by clays, being degraded by microbes and its cost (SATTER; IQBAL, 2016; VISHNYAKOV *et al.*, 2020).

Another chemical flooding used is micellar polymer, where higher concentrations of surfactant are injected and combined with incompatible polymers, and micellar solutions establish viscosity. Micellar polymer flooding has a complicated design process, usually including the injection of a prewash (water or alkaline) and a post-wash of the polymeric solution followed by water, and although this flooding complexity, in the 70s and 80s, many fields employed it (WYATT *et al.*, 2008; SATTER; IQBAL, 2016).

The efficiency of this process is associated with its ability to reduce interfacial tension and improve injected fluid mobility. It also has the advantages of promoting oil solubilization and oil-water emulsification. As discussed, this flooding is complex and restricted, quoting: its properties have sensitivity to certain conditions (salinity, temperature, etc.), and its application is nearly restricted to light oils, homogeneous rock, and high-area sweep reservoirs (WYATT *et al.*, 2008; SATTER; IQBAL, 2016).

Alkaline flooding, another chemical EOR process, also has a mechanism based on surfactants' action. However, surfactants are the product of a reaction between injected fluids (sodium hydroxide, sodium carbonate, and sodium silicate solutions) and organic acids in the oil. Chemical products react with the reservoir system, reducing oil/water interfacial tension and creating a lower viscosity emulsion, and act with the rock, changing its wettability. The first application of alkaline flooding in reservoirs was performed in the '40s, and its use has increased since then, mainly in those with considerable amounts of polar active compounds, despite their limitations and sensitivities with the oil °API and reservoir heterogeneities (SATTER; IQBAL, 2016; VISHNYAKOV *et al.*, 2020).

### 2.3.3 Nanoparticle injection

One of the main goals of the petroleum industry is the recovery rate improvement, which has accelerated the development of new technologies to increase oil extraction with greater feasibility (SMALLEY *et al.*, 2009As referred, the Enhanced Oil Recovery stage (EOR) covers a wide range of methods such as gas injection, polymer, surfactants, and alkaline flooding, which have shown efficiency in increasing production rate. Additionally, recent studies showed the potential of nanotechnology innovations, with outcomes in rock wettability modification and interfacial tension alteration between oil and other reservoir fluids (GUO *et al.*, 2016; ALI *et al.*, 2018).

Nanoparticles, such as nanoemulsions and nanoclays, are distinguished nanomaterials classified by their shape and structure. The nanoparticles are, in particular, found in nanocomposite structures or formats ranging in size from 1 to 100 nm, having unique properties due to their size. It has therefore been considered suitable for EOR application and also extensively researched. Currently, the nanoparticles for nanoflooding so far studied may have an organization based on three categories, metallic oxides (*e.g.* $Al_2O_3$, CuO, $Fe_2O_3$, $Fe_3O_4$, $Ni_2O_3$, $TiO_2$), organic (*e.g.* carbon nanoparticles and nanotubes) and inorganic (*e.g.* $SiO_2$). Mechanisms of action include interfacial tension (IFT) and viscosity reduction, change in wettability to foam, and emulsion stability (NEGIN; ALI; XIE, 2016; SIRCAR, 2020).

Silica nanoparticles are one of the most promising technologies for EOR application in the pore space through entrapped oil remobilization. Its effective action occurs by changing the interfacial tension between the phases (solid/liquid/liquid), altering the rock wettability, or even creating a breakdown pressure at the oil-rock interface (ALI *et al.*, 2018; HENDRANINGRAT; LI; TORSATER, 2013).

To investigate only silica nanoparticle (SiN) mechanisms of action, without using surfactants or stabilizers to make the suspension, JIANG, LI, and HORNE (2017) evaluated and isolated their effects on wettability alteration (through contact angle measurements) and IFT reduction. They found out that silica nanoparticles have an influence on changing wettability but not on reducing the IFT. In addition, the authors performed core flooding experiments using nanoflooding with different SiN diameter sizes, observing an increase in the recovery factor, then indicating that wettability

alteration undergoes influence by nanoparticles but not concluding the relation of SiN size with this increase.

JIANG, LI, and HORNE's (2017) research concerns were the effect of the nanoparticles alone in improving the oil recovery rate, while LI *et al.* (2018) implications were the recovery experiments upon harsh reservoir conditions, showing the need for a stabilization agent for SiN flooding. Due to its surface charges, silica nanoparticles possess an agglomeration and adsorption tendency; to overcome this, LI *et al.* (2018) and co-workers used HCl to promote a stable nanoparticle suspension. Conducting the same experiments (contact angle and IFT), they reach the same conclusion as JIANG, LI, and HORNE's (2017) work.

With the same reservoir conditions (high salinity, temperature, and pressure) as LI *et al.* (2018), PATEL *et al.* (2017) also used a stabilizing agent for SiN, an anionic surfactant. In the presence of two immiscible fluids, such as those found in the reservoir, the IFT between the fluids generally decreases, creating an in-situ emulsion. The studies carried out by the authors demonstrate that commercial SiN alone indeed forms this kind of emulsion in light oil. Unlike LI *et al.* (2018) and JIANG, LI, and HORNE (2017), the authors' results showed that SiN and SiN with surfactant lower the IFT between oil and synthetic brine, where surfactant alone was unable, but they did not perform displacement experiments.

As for the study conducted by ROSTAMI *et al*. (2020), making the same evaluation as JIANG, LI, and HORNE (2017) about the effect of the nanoparticles alone, they reached a similar result regarding wettability alteration but not for IFT, which was found that silica nanoparticles (SiN) have a slight influence on changing it. The authors also did, in the SiN, a stability test and a flow experiment in a salinity environment. The flooding performed in a glass micromodel shows that both displacement tests (with and without salt) increased the recovery factor and remained stable, especially in salinity conditions.

WANG *et al*. (2018) used silica nanoparticles no-modified/modified to be hydrophobic and dispersed in water with surfactants for stability. Their contribution was focused on the mechanisms of wettability alteration (contact angle and adhesive force) and core flooding experiments. The study findings were that the SiN is stable with surfactants, and a better recovery factor was achieved with it than with only a surfactant

solution. The contact angle results corroborate this oil displacement increase, whereas the adhesive force measurements were inconclusive.

TABLE 2.1 shows a resume of these cited papers, correlating their main parameters studied, conditions, and findings.

TABLE 2.1 – Resume of the correlated papers in silica nanoparticle EOR.

| Autor | Parameters Evaluated | Conditions | Findings |
|---|---|---|---|
| JIANG, LI and HORNE (2017) | Wettability alteration, IFT reduction and recovery factor | Without surfactants or stabilizers to make the suspension; different SiN diameter sizes | Have influence in changing the wettability, but none in reducing the IFT. No relation in the SiN size with this increasing in recovery factor |
| LI *et al.* (2018) | Wettability alteration and IFT | Harsh reservoir conditions; stabilization agent | Have influence in changing the wettability, but none in reducing the IFT. |
| PATEL *et al.* (2017) | IFT | Harsh reservoir conditions; stabilization agent | SiN and SiN with surfactant lower the IFT |
| ROSTAMI *et al.* (2020) | IFT, wettability alteration, NP stability and recovery factor | Without stabilization agentes; salinity environment | Have influence in wettability alteration and little in IFT reduction; stability and good recovery factor in salinity environment |
| WANG *et al.* (2018) | Wettability alteration and recovery factor | With stabilization agent; SiN modified | Stable SiN with surfactants and better recovery factor achieved with it than only surfactant |

SOURCE: AUTHOR (2022)

## 2.4 X-RAY MICRO-COMPUTED TOMOGRAPHY ($\mu$CT)

X-ray computed tomography has been mainly used for modern diagnostics in medical radiology to obtain three-dimensional (3-D) images. Later, in a different application area, X-ray CT started to be used in material sciences as a nondestructive test for safety inspection of airplanes, turbines, engines; to analyze 3-D volumes of biological and geological samples, for metrology, and for quantitative experiments, due to its image quality, its resolution range varies from micro to nanometers and for being a nondestructive technique (HANKE *et al*., 2016; PETH, 2010).

The principles of computerized tomography technique are based on X-ray attenuation differences when they pass through an object, which can be absorbed or scattered by matter, the theories that describes these two processes are called Compton and photoelectric effects, respectively. The photoelectric effect, in the energy range normally available in synchrotron laboratories and benchtop equipment, is predominant and consists of the transmission of all the energy of the incident photon to an internal electron of an atom, where the electron partially uses this energy to overcome the energy bond, then being removed from the atom, this effect is a function of the effective atomic number. Compton effect is an interaction of X-ray photons with free or weakly bound electrons that are scattered and with a little energy loss (ARCHILHA, 2015). The relationship between the initial number of incident photons (N0) and the number of transmitted photons (N) in a homogeneous object is given by the Lambert-Beer's law (KAK; SLANEY, 1988):

$$N(x) = N_0 e^{-\mu x} \tag{2.12}$$

where μ is the overall linear attenuation coefficient and x is the sample thickness.

The Equation (2.12) is applicable if the incident photons are monochromatic. If the sample is composed by different materials and by considering a non-monochromatic X-rays, there is a broadband spectrum energy distribution, the last equation become Equation (2.13), where μ is also a function of energy (E):

$$N(x) = \int_0^{E_{max}} N_0(E) e^{-\int_0^x \mu(\eta)\, d\eta} dE \tag{2.13}$$

where η is the rate of energy loss due to the photoelectric and Compton effect.

The tomographic technique for acquiring 3-D images basically works with the use of a suitable X-ray source (X-ray tubes or synchrotron) to beam generation, where it passes through an object, positioned in front of a detection device and several 2-D radiographs are taken during a 0-180º or 0-360º rotation of the sample and, after a reconstruction process, a 3D sample image representation is obtained for further studies (FUSSEIS, 2014; HANKE *et al*., 2016).

The reconstructing process is computationally expensive and, ideally, it is performed on powerful computers (clusters). The most used reconstruction algorithm is filtered-back-projection (FBP), which uses the 'Randon transform' to convert 2D projections into a 3D image (HANKE *et al*., 2016; KAK; SLANEY, 1988). When the Randon transform of a line of 2-D image projection pixels (that is, a certain height of the image in the detector) as a function of rotation angle is displayed as an image (FIGURE 2.4, b), we have what is called sinogram and it has the necessary data to reconstruction (GONZALES; WOODS, 2002).

FIGURE 2.4 – (a) Intensity signal recorded from a 2-D model, in certain angle (ω), along the corresponding pixel row of the detector (marked by a yellow line). (b) Sinogram generated by applying a Radon transform to the same pixel row at different rotation angles.

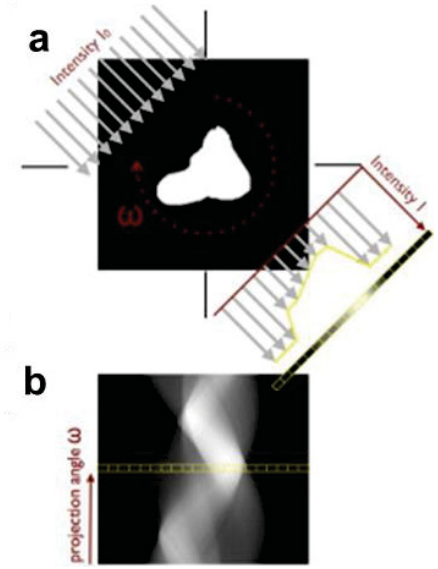


SOURCE: MODIFIED FROM FUSSEIS (2014).

To obtain a 3D tomography using FBP, it is necessary to stack all slices (2D image), after being reconstructed from each sinogram generated from image. The reconstruction of an image slice is shown in FIGURE 2.5, where for each angle recorded, a retro projection of the radiographic absorption profile, of a pixels' row, is added to the image space. In FBP reconstruction methods, the more projections at different rotation angles ($\omega_n$), the more the final results resemble the original image (FUSSEIS, 2014; WILLMOTT, 2011).

FIGURE 2.5 – Illustration of filtered back projection reconstruction at different rotation angles of the sample.

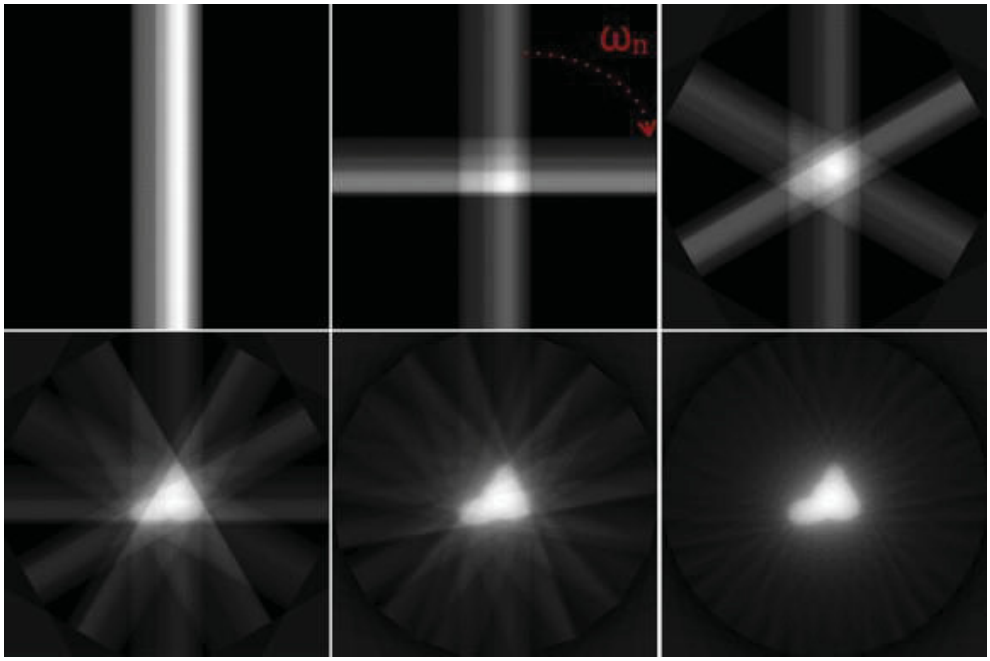


SOURCE: FUSSEIS (2014)

X-ray micro-tomography ($\mu$CT), in material sciences, is done in synchrotron facilities or by benchtop scanners, they do not differ much in terms of image acquisition, the main difference is the x-ray source. The schematic diagram of these two scanning devices is shown in FIGURE 2.6 In the laboratory scanner, the rotating sample is located between an X-ray tube, which generates poly-chromatic beam, and the detector (FUSSEIS, 2014).

The beam generated in the synchrotron (energy source) passes through an optional monochromator device and hits the rotating sample. The transmitted beam is acquired by the detection system, which can be either a direct system with an area detector sensible to X-rays or an indirect system, where a scintillator first converts X-rays into visible light and then is captured by an CMOS/CCD-based detector. In synchrotron based $\mu$CT, the data acquisition is faster than in laboratory based; besides that, it has better resolution and the advantage of using a monochromatic beam, which improves image quality (FUSSEIS, 2014).

FIGURE 2.6 – Schematic layout of a benchtop scanner (a) and of a Synchrotron μ-tomography beamline (b).

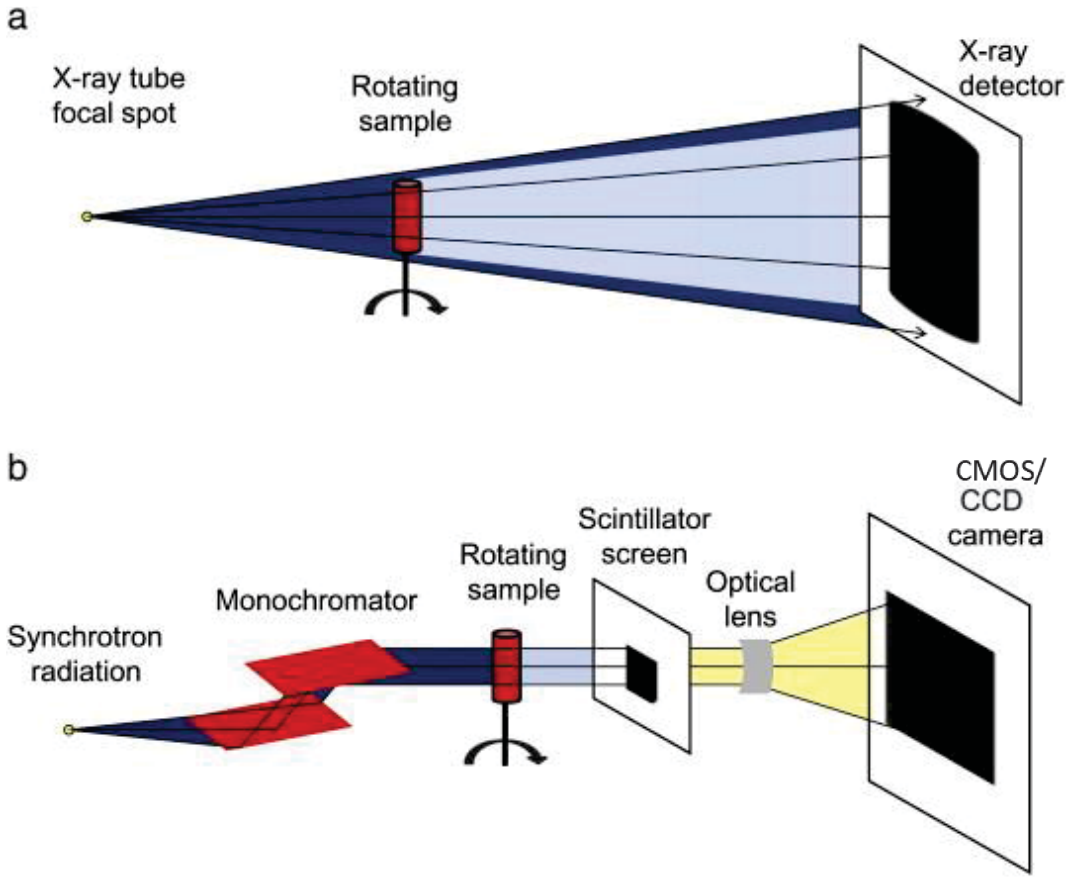


SOURCE: CNNUDE; BOONE (2013).

# 3 METHODOLOGY

## 3.1 OIL RECOVERY EXPERIMENTS

To better understand the action of silica nanoparticles in oil recovery, this study was divided into two phases. In the first phase of flow experiments, the nanoparticles' action in EOR was evaluated in different concentrations and sizes. To study this, the chosen porous material was glass beads of a known size (<150 mm) to mimic the porous space of rock.

For the second phase flow experiments, for a better investigation of nanoparticle action, an unconsolidated oolitic limestone (ooids from Turks and Caicos) was used, as a representative for carbonate reservoir rocks. Here, the SiN performance was analyzed in more realistic conditions and explored the SiN size that presented the best efficiency. Samples were prepared in the same way described in the first phase.

Beyond the different porous materials used, in the first phase, for image acquisition it was used a synchrotron x-ray source and microtomographic equipment available at IMX Beamline in CNPEM facilities. Also, the nanoparticles used were synthesized and characterized by researchers at the Nacional Laboratory of Nanotechnology (LNNano) in CNPEM.

As for the second phase, for image acquisition it was used a benchtop scan, available at the LAMIR laboratory on the UFPR campus, and the nanoparticles were synthesized using the same procedure and characterized by researchers of this present work. TABLE 3.1 summarize the specificities of each phase.

TABLE 3.1 – Specificities of each flow phase experiment

| **Experiment Phase** | **Porous samples** | **Phase specificities** | | |
|---|---|---|---|---|
| | | Porous medium material | X-ray source | Silica nanoparticles (synthesis and characterization) |
| *First Phase* | Core 1<br>Core 2<br>Core 3 | Glass beads | Synchrotron | Researcher of the LNNano |
| *Second Phase* | Core 4 | Oolitic limestone (ooids) | X-ray tubes | Authors |

SOURCE: AUTHOR (2022)

## 3.2 SILICA NANOPARTICLE SYNTHESIS

Silica nanoparticle (SiN) synthesis was carried out following a modified Stöber method (LEE; BEYER; FURST, 2005). Briefly, the reactional medium was prepared with 120 mL of ethanol (EtOH P.A., Merck) and appropriated quantities of ammonia ($NH_4OH$, 28 - 30 m %, Sigma Aldrich), related in TABLE 3.2. The result solution remained in constant stirring for 30 minutes. In this reaction, ammonia was the catalyst and also the determining of nanoparticle (NP) size.

TABLE 3.2 – Relationship between the amount of ammonia and the nanoparticles size

| Nanoparticle | Diameter of interest (nm) | Ammonia quantity (mL) |
|---|---|---|
| SiN-30 | 30 | 3,5 |
| SiN-60 | 60 | 4,5 |
| SiN-100 | 100 | 5,5 |

SOURCE: AUTHOR (2021)

After that, were added to the stirring solution, two aliquots of 2.5 mL of TEOS (Tetraethyl orthosilicate – Sigma Aldrich) were added, as silicon source and precursor, with 3 hours of an interval between the aliquot addition. The reaction continued overnight under stirring at room temperature.

SiN-100 was purified by centrifugation (10,000 RPM, 20°C and 15 minutes), washed once in EtOH P.A., and then four times in water. The nanoparticle resuspension was done by sonication for 30 minutes after centrifugation at each purification step. SiN-30 and SiN-60 were purified by dialysis (hydrated cellulose membranes MWCO = 14,000 Da) using ethanol: water 1:1 solution (two changes every 12 hours) and pure water, deionized water 18.2 MΩ.m, purified in Milli-Q system, (four changes every 12 hours).

## 3.3 NANOPARTICLE CHARACTERIZATION

The following technique was used to characterize the silica nanoparticle synthetized:

DLS and Zeta Potential: Dynamic light scattering (DLS) measurements were performed on a Malvern Zetasizer ZS (Malvern Instruments, UK) equipped with a red laser (632.8 nm) and operating in backscattering mode with a detection angle of 173°.

NP sizes and size distributions were calculated by Malvern Zetasizer Software from three measurements per NP sample (1 mg $mL^{-1}$), each one consisting of 10 runs of 10 seconds at 25 °C. The determination of surface charge of the nanoparticles, by means of Zeta potential (ZP) measurements, was performed on a dispersion of NPs (1 mg $mL^{-1}$) in water at 25 °C on the same equipment.

SEM: NP scanning electron microscopy (SEM) analysis was carried out with a JEOL 6010LA microscope operating at an accelerating voltage of 20 kV to investigate nanoparticles size and morphology. NPs 2.5 $mg.mL^{-1}$ suspensions were dropped over a copper substrate, dried under room temperature, and Au and Pd sputter-coated in a Denton Vacuum Desk V equipment.

Gravimetric determination: NPs concentration ($mg.mL^{-1}$) in the purified suspensions were gravimetric determined by weighing the remaining solid after water removal by heating.

## 3.4 POROUS AND FLUIDS SAMPLES CHARACTERISTICS

The porous samples were prepared using a cylindrical plastic tube with a 3 cm inner diameter, filled with the corresponding material of each phase. Used different cores for each nanoparticle solution injection, as shown in FIGURE 3.1; furthermore, the physical properties of each core sample were described in TABLE 3.3.

FIGURE 3.1 – Packed glass bead sample for use in the flow cell

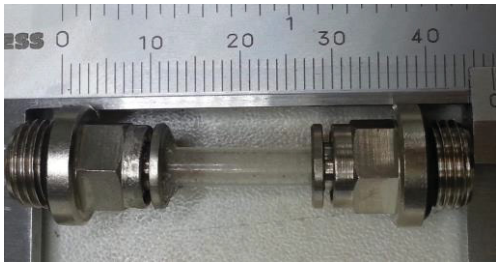


SOURCE: AUTHOR (2021).

TABLE 3.3 – Physical properties of core samples

| | Porous Sample | Porosity (%)* | Permeability (mD)** |
|---|---|---|---|
| **First Phase** | Core 1 | 27 | 202,97 |
| | Core 2 | 30 | 304,46 |
| | Core 3 | 33 | 101,49 |
| **Second Phase** | Core 4 | 40 | 91,34 |

*Calculated by the software AVIZO, using the segmented image;
**Calculated based on Darcy's Law

SOURCE: AUTHOR (2022).

For the simulation of the recovery phases of an oil reservoir, the following fluids were used:

Water: Deionized water 18.2 MΩ.m, purified in the Milli-Q system, was used for nanoparticle synthesis and waterflooding injection simulation.

Oil: A solution composed of 65% dodecane and 35% 1-iododecane was prepared to aim for better x-ray attenuation during the tomography measurements. Both are mineral oils with a density close to water density, avoiding gravity-driven separation.

Nanoparticle solution: For each nanoparticle size (30, 60, 100 nm) dilutions were made, in a concentration of 0.05 and 0.1 wt%, with deionized water, in the first phase experiment. And for the second phase experiment, the SiN-100 nm was used in 0.1, 0.2, and 0.3 wt% concentrations.

## 3.5 EXPERIMENTAL FLOW SET-UP

Flow cell: For the simulation of oil recovery in a porous medium, a flow cell and an injection system with software controlling were used, (FIGURE 3.2) both developed by the IMX Beamline staff at CNPEM (COSTA, 2022). The injection system (in blue) consists of three syringes, which makes the fluids of interest injection directly below the sample (in red).

FIGURE 3.2 – Flow cell and experimental set-up scheme of oil recovery simulation.

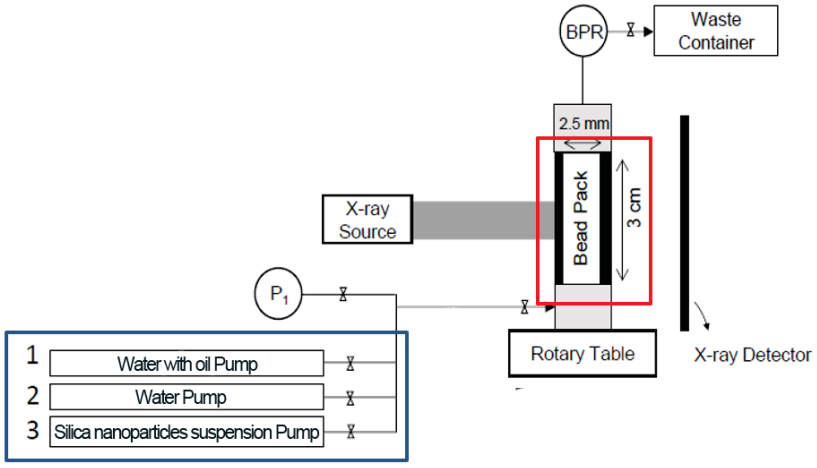


SOURCE: AUTHOR (2021).

The porous space sample selected (FIGURE 3.1) is coupled to the flow cell, which was designed to allow even three fluid injections. In the existing system fluid, a 40 psi backpressure regulator (FIGURE 3.2 – BPR) was installed, avoiding the formation and propagation of bubbles in the porous sample and injection system. The same setup was used in both phases; the only difference is that in the second phase of the experiment, the flow cell was installed apart from the microtomography scanner.

Firstly, were made a water injection until complete saturation of the medium, followed by a fast x-ray microtomography scan to evaluate the system in the absence of gas (bubbles). At this point, the permeabilities of the porous spaces were measured upon different flow rate injections (Darcy's Law) using a pressure sensor (FIGURE 3.2 – $P_1$). After the permeability measurement, the system was flooded with oil to simulate the initial reservoir conditions. As for the different oil recovery stages simulation, the water was injected initially, followed by nanoparticles suspension solution, in distinct concentrations. The injection conditions are presented in TABLE 3.4 and TABLE 3.5, each for its respective experimental phase.

### 3.5.1 Microtomography Measurement

First phase experiment: Tomography image acquisitions were made after each fluid injection, related in TABLE 3.4, in a Synchrotron X-ray microtomography (μCT) beamline.

TABLE 3.4 – Injection conditions for the experimental set-up of the first phase

| Fluid | q (μl/min) | Injected pore volumes | BPR (psi) |
|---|---|---|---|
| Initial water | 100-700 | >10 | 40 |
| Oil | 100 | 10 | 40 |
| Water | 10 | 10 | 40 |
| SiN – 0.05 wt% | 10 | 10-15 | 40 |
| SiN – 0.1 wt% | 10 | 10-15 | 40 |

SOURCE: AUTHOR (2021).

The μCTs measurements were conducted at IMX Beamline from Brazilian Synchrotron Light Laboratory at CNPEM (FIGURE 3.3). The detection system is composed of LuAg:Ce scintillator, which transforms x-ray into visible light, one objective for image magnification (in this experimental case, it was used a 5X objective lens), and one CCD camera (pco.2000), with 2048 x 2048 pixels, the pixel size is 7.4 x 7.4 μm. Binning function was activated in the camera, allowing it to double the pixel size, lowering the exposure time by four times. Aiming to perform a fast (~minutes) scan during fluid injections. While the sample rotated 180°, were captured 1024 2D images (projections) to generate 3D images, with ~1 s of exposure time per projection. Data reconstruction, *i.e*. 2D data set transformation in tridimensional data, was made using the RAFT (MIQUELES; KOSHEV; HELOU, 2018).

FIGURE 3.3 – Experimental set-up installed at CNPEM's IMX Beamline. The injection system (in blue) is composed of three syringes, which inject the fluids of interest directly underneath the sample (in red).

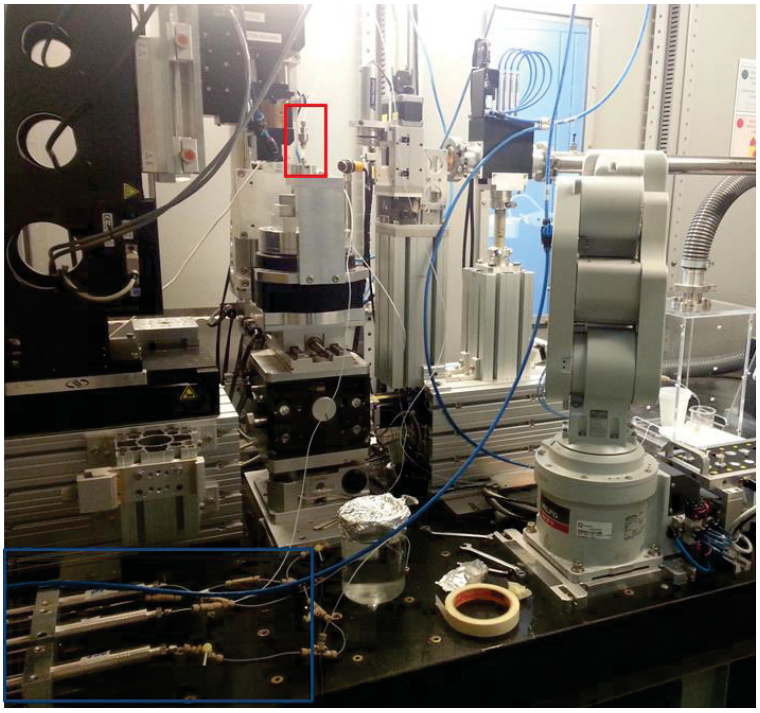

SOURCE: AUTHOR (2022).

Second phase experiment: Tomography image acquisitions were made after each fluid injection, related in TABLE 3.5, using a benchtop X-ray microtomography equipment.

TABLE 3.5 – Injection conditions for the experimental set-up of the second phase

| Fluid | q (µl/min) | Injected pore volumes | BPR (psi) |
|---|---|---|---|
| Initial water | 100-700 | >10 | 40 |
| Oil | 100-700 | >10 | 40 |
| Water | 31 | 10 | 40 |
| SiN – 0.1 wt% | 31 | 10-15 | 40 |
| SiN – 0.2 wt % | 31 | 10-15 | 40 |
| SiN – 0.3 wt % | 31 | 10-15 | 40 |

SOURCE: AUTHOR (2022).

The µCTs measurements were conducted at LAMIR laboratory on the UFPR campus (FIGURE 3.4 - B), using the microtomography equipment SkyScan 1172. A 100 kV and 100 µA X-ray source was used, with a 0.5 mm aluminum filter, and with a rotation step of 0.25°, during image acquisition, captured 2441 2D images (projections)

to generate 3D images. An 11-megapixel camera was used, for image detection, with 4000 × 4000 pixels. Data reconstruction was due with the SkyScan NRecon software.

FIGURE 3.4 – Experimental set-up installed at UFPR. (A) Flow cell and syringes pump, (B) SkyScan 1172 microtome

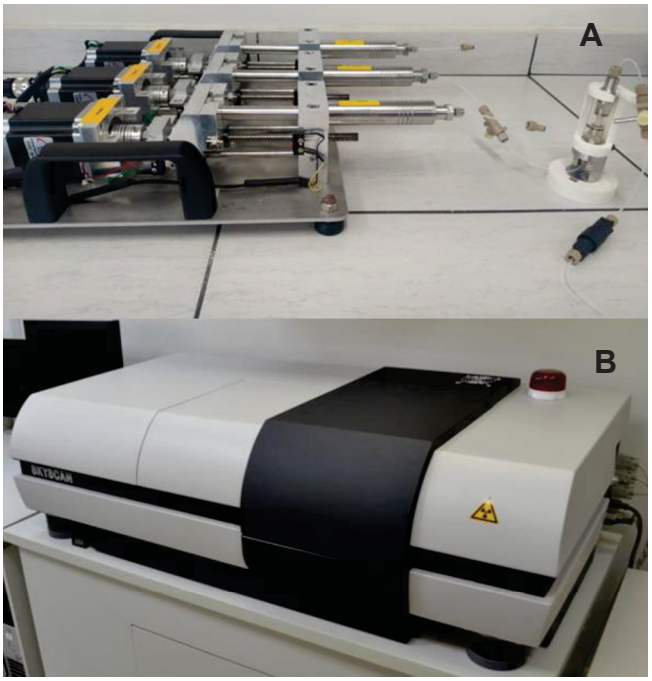


SOURCE: AUTHOR (2022).

µCT Data processing: µCT generated data was processed by segmentation using the Weka plugin, a U-Net network (deep learning) and the AVIZO 9.7 software (FIGURE 3.5). Also, this last software was used for the quantification of each fluid/solid phase present in reconstructed images (3D images).

FIGURE 3.5 – 3D images processing flowchart, generated through µCT

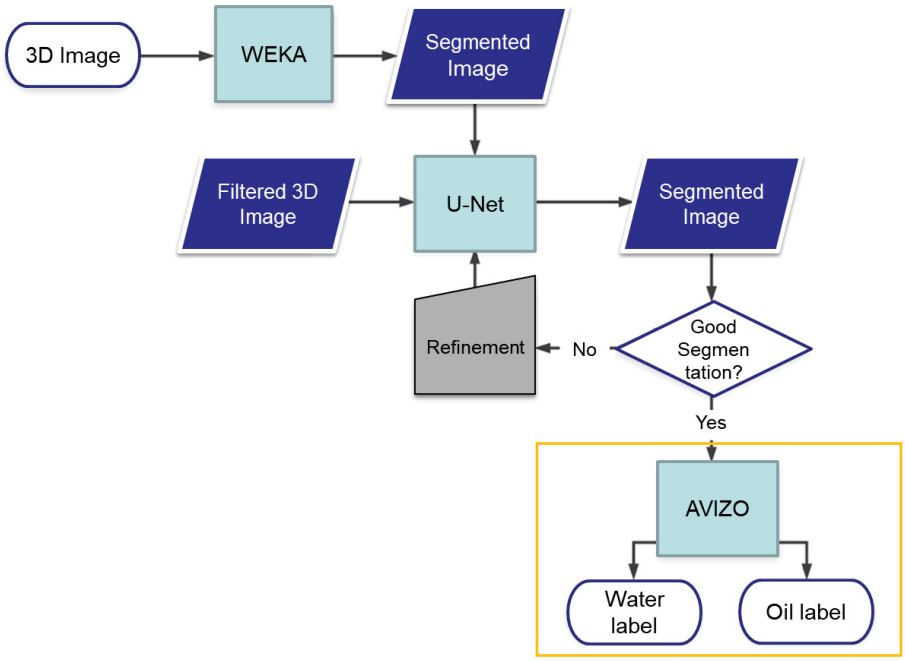


SOURCE: AUTHOR (2021).

As a first step, it was used the Trainable Weka Segmentation, or simply Weka, a 3D image segmentation plugin available in Fiji that relies on the combination of machine learning algorithms and image feature identification. In this step, the training of a classifier by deploying seeds for machine learning was performed, separating the image into two labels only, focused on identifying the beads.

The masks resulting from this process, after minor manual corrections, together with the original filtered image, were used as input data for the refinement of a network previously trained by the researcher's segmentation experts at the Scientific Computing Group (GCC) of CNPEM, for the classification of similar images. This network was used only for the glass beads segmentation from the first phase results.

At least, in the AVIZO 9.7 software, using the mask of the glass beads created, this was removed from the final image using the multiply by image tool, which allows the multiplication of a mask (a binary image composed of 0 and 1). Then, it was possible to individualize oil and nanofluid (or water) phases using tools such as threshold and watershed.

For the second phase of experiment result segmentation, were used the tools available on AVIZO for the rock mask creation, and after only this last step, using the software (FIGURE 3.5 orange square) was applied.

# 4 RESULTS AND DISCUSSION

Once the experimental phases, exposed and explained in FIGURE 4.1, were completed, the results were arranged and presented throughout this topic through tables, graphs, slices, and 3D rendering figures, for the system studied experimentally.

FIGURE 4.1 – Experimental phases flowchart

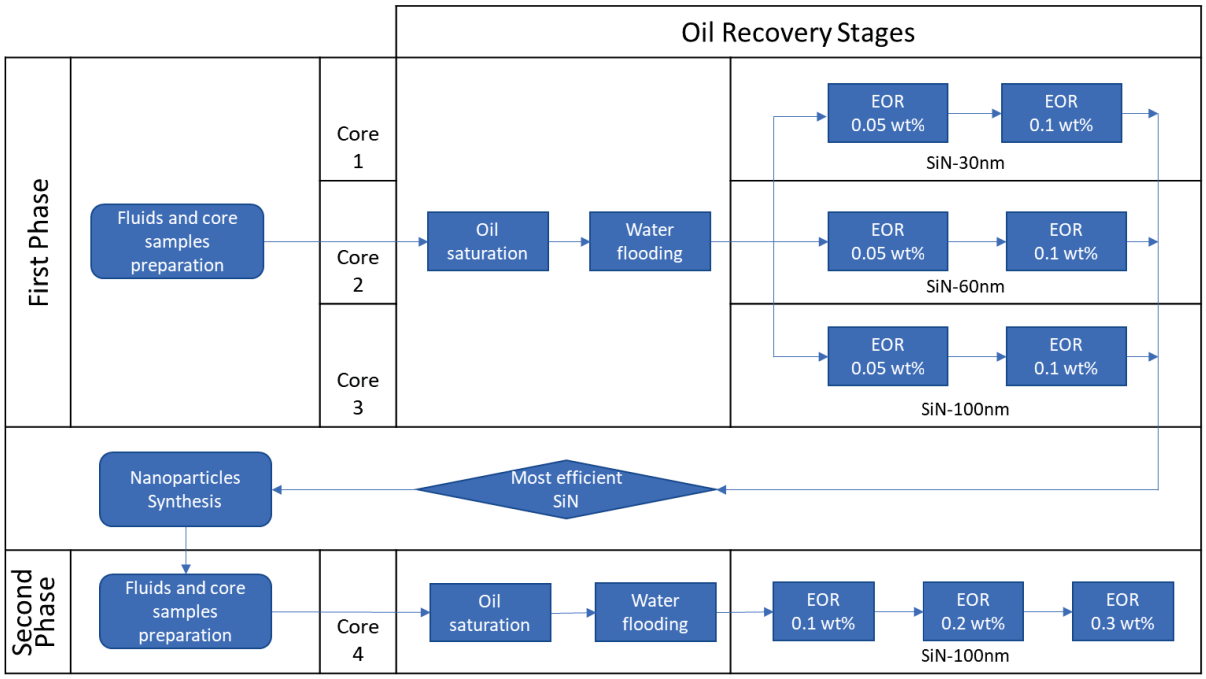


SOURCE: AUTHOR (2022).

## 4.1 FIRST PHASE EXPERIMENTS

In order to evaluate the recovery efficiency and oil remobilization, the same slice was selected (2D image of a 3D image in xy coordinate) in the different recovery stages. In FIGURE 4.2, the oil volume can be followed in the same spot in each porous sample along the flow experiments.

FIGURE 4.2 – Images of oil saturation and recovery steps, using nanoparticles of 30 (A), 60 (B) and 100 (C) nm in diameter in the EOR. Scale represents 300 μm

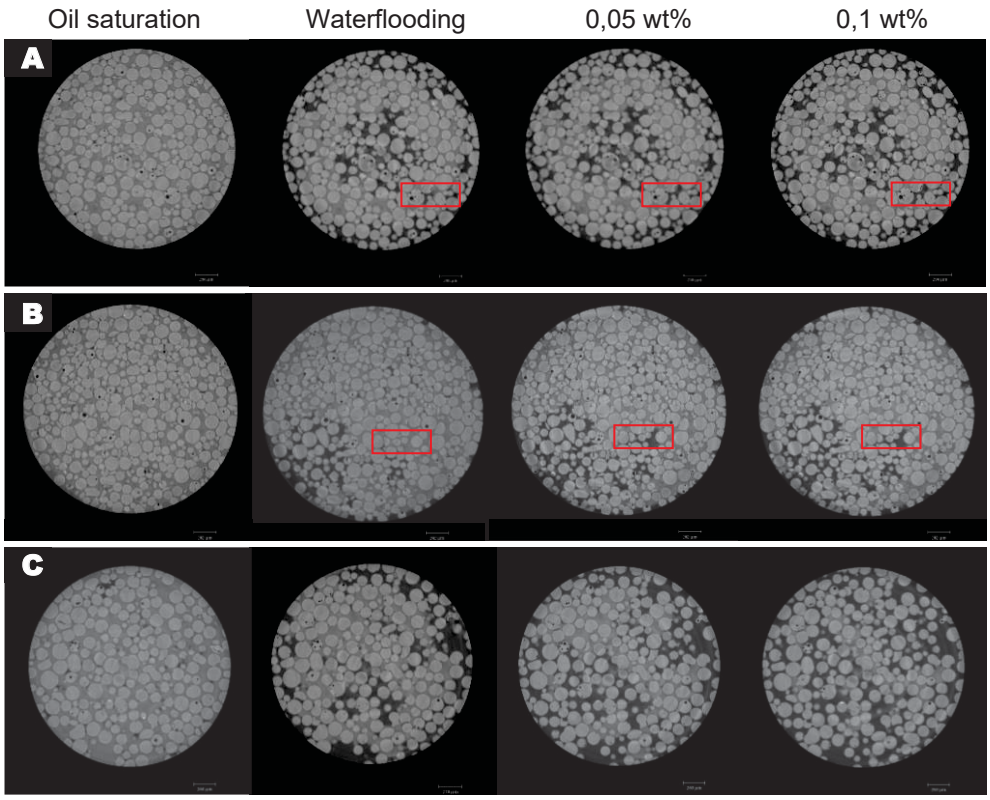


SOURCE: AUTHOR (2021).

Analyzing the silica nanoparticles (SiN) of 30 nm and 60 nm slices studied, the oil phase remains almost the same. Slight changes between the stages that can be noticed (in red contour) are more related to the remobilization of oil in pores than to the recovery of it. FIGURE 4.3 demonstrated the quantitative evaluation of oil volume in each recovery stage, where the result of these two SiNs indeed didn't show efficiency in decreasing the oil saturation. Nevertheless, based on 2D and volume analyses, the experiment using SiN of 100 nm presented recovery action on the oil trapped in porous media after the waterflooding.

FIGURE 4.3 – Recovery efficiency graph using NP of 30, 60 and 100 nm at different concentrations (0.05 and 0.1 wt%)

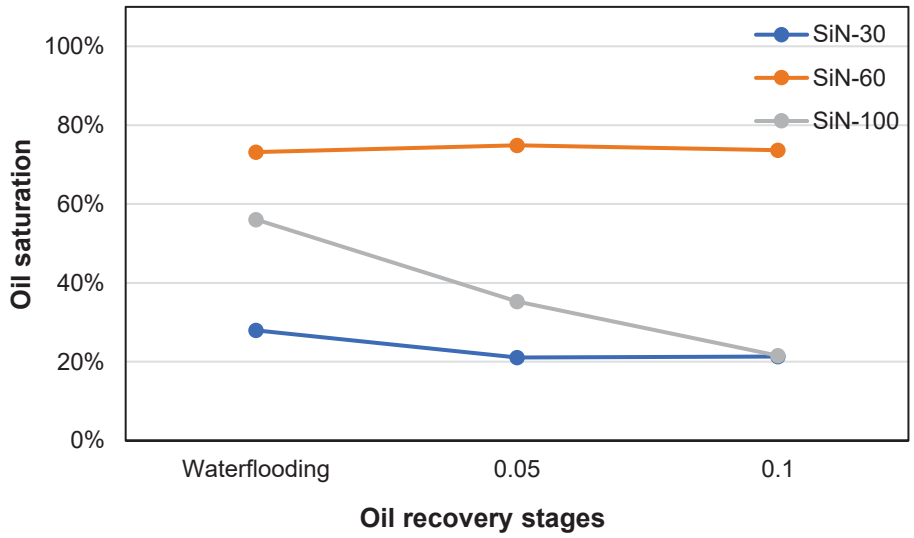


SOURCE: AUTHOR (2021).

Even though the experiment conducted with the nanoparticle of 30 nm had removed more oil them the one with 60 nm, this cannot be associated with the effect of SiN size increase, but, actually, this volume quantity is due to the highest percentage already recovered in waterflooding stage.

After nanoparticle injection at 0.05 wt% concentration, the SiN-30 removed 7% of the remaining oil after the waterflooding, while SiN-60 for the same concentration experiment had a saturation increase of 2%. In 0.1 wt% concentration nanoflooding, 1% of the remaining oil from the early stage was removed using SiN-60, where the SiN-30 had a volume increment in the same proportion; 3D volume rendering reinforces this evidence (FIGURE 4.4 and FIGURE 4.5).

FIGURE 4.4 – 3D rendering of oil volumes in the recovery steps, using 30 nm silica nanoparticle in the EOR. (A) initial oil saturation, (B) waterflooding, nanoflooding (C) 0.05 wt% and (D) 0.1wt%.

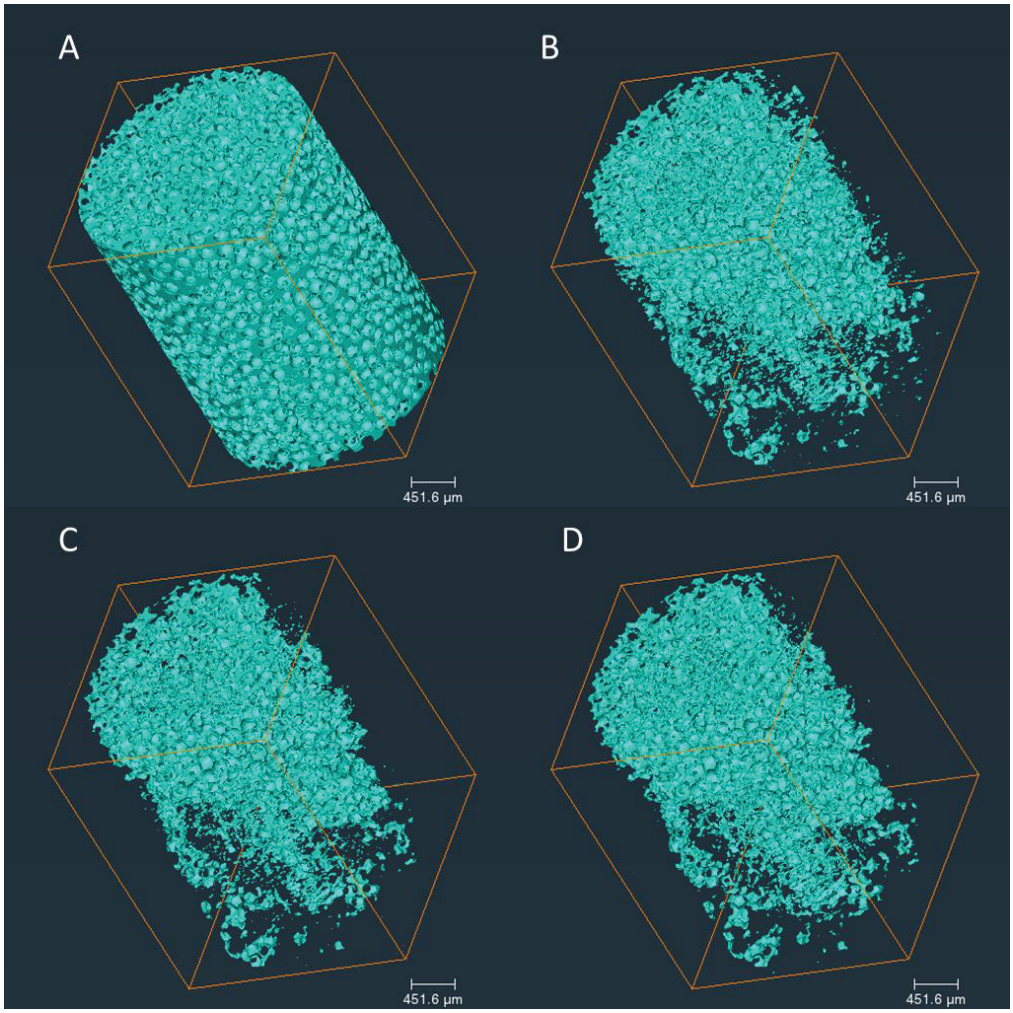


SOURCE: AUTHOR (2022).

This oil saturation increment during the nanoflooding could be explained, as previously mentioned, by the oil remobilization from the sample bottom, which was out of the field of view (FoV), thereby, an oil volume mobilization occurs in the section where quantification analyses were done.

Pak *et al*. (2018) in their study also did not observe a difference in the final oil saturation after flushing the core with a 30 nm nanoparticle suspension, like our experiment with SiN of 60 nm. But they report an active SiN remobilized action inside porous space. This oil dynamic in the pores is associated, as already reported (PATEL *et al*., 2017; LI; TORSÆTER, 2015; PAK; ARCHILHA; AL-IMARI, 2018; KEYKHOSRAVI *et al*., 2021), with the decreasing IFT due to nanoparticles action as a surfactant, reduction the capillary force that retains the oil to rock surface.

FIGURE 4.5 – 3D rendering of oil volumes in the recovery steps, using 60 nm silica nanoparticle in the EOR. (A) initial oil saturation, (B) waterflooding, nanoflooding (C) 0.05 wt% and (D) 0.1wt%.

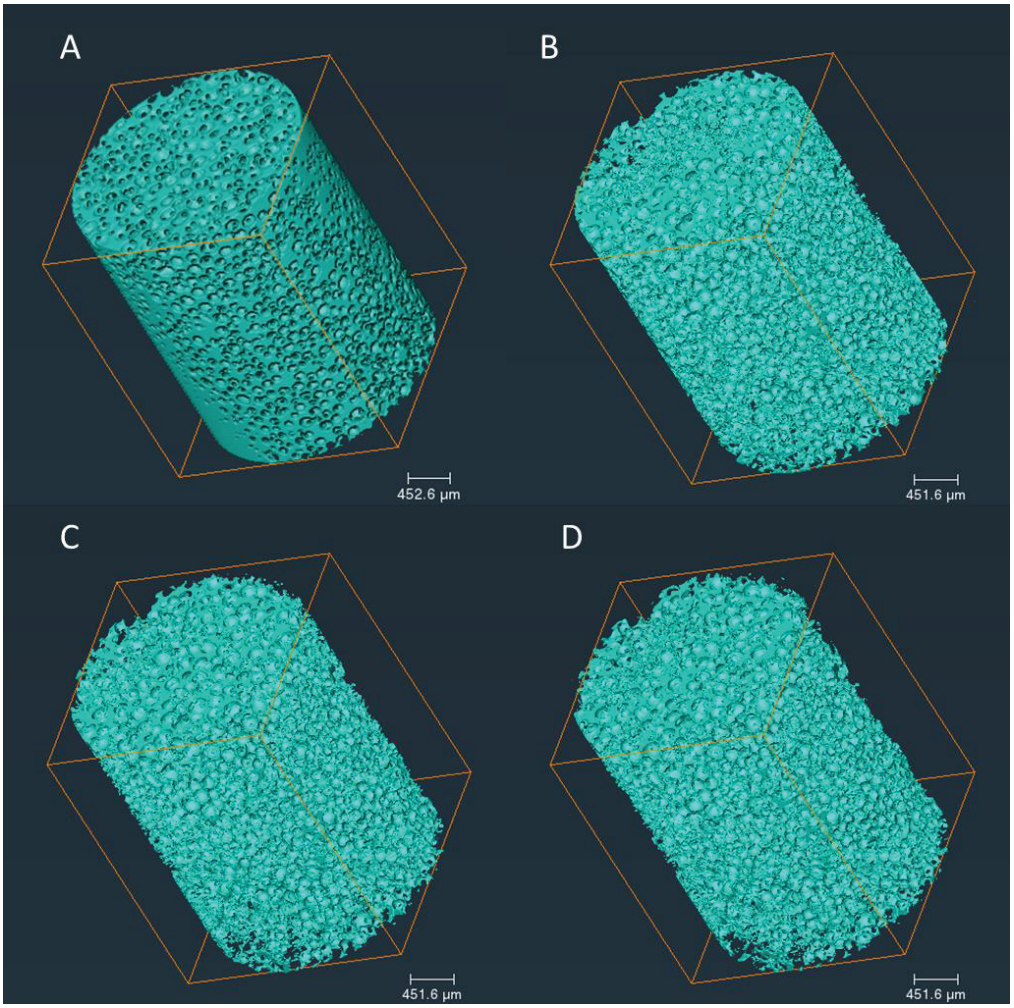


SOURCE: AUTHOR (2022).

The SiN-100 experiments, differently from the others presented, had an increase in initial oil volume recovered from 44% after waterflooding to 65% and then to 78% after nanoflooding, starting with the lower concentration. This efficiency is highlighted by the 3D volume rendering of oil amount in each recovery stage, (A) initial oil saturation, (B) waterflooding, (C) and (D) nanoflooding at a distinct concentration (FIGURE 4.6).

In the study conducted by HENDRANINGRAT, LI, and TORSATER (2013), silica nanoparticles with smaller sizes presented better remobilization and oil recovery effect, as long as in this experiment, the opposite was found, the largest nanoparticle showed more efficiency.

FIGURE 4.6 – 3D rendering of oil volumes in the recovery steps, using 100 nm silica nanoparticle in the EOR.

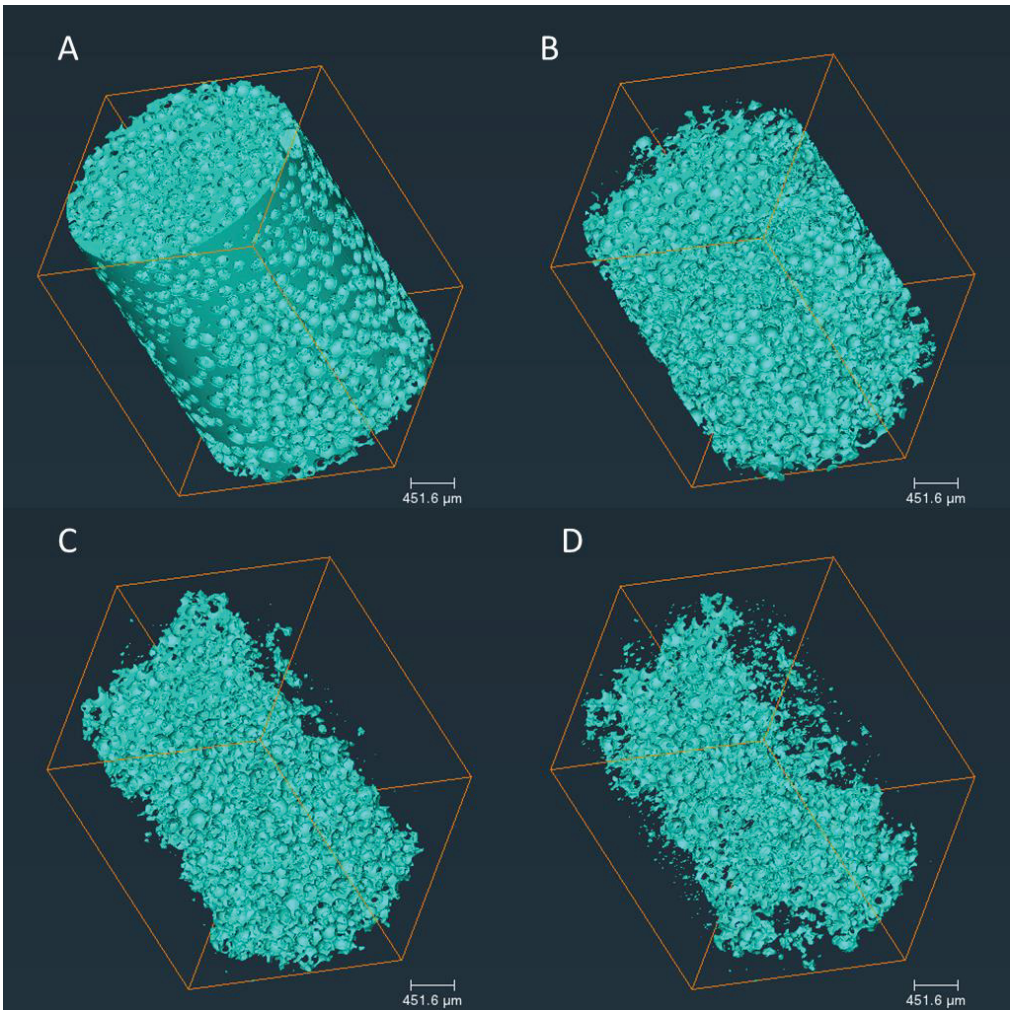


SOURCE: AUTHOR (2022).

Analyzing the physical properties of the core samples (TABLE 3.3), in this first stage was observed that the higher permeability value lowest the recovery percentage. It can be explained by the needed time to SiN act inside the porous medium, since the fluid flow less easily in lower permeability, there is time for the nanoparticle to retain in the oil/rock interface and form a stable wedge film and perform its mechanisms. KEYKHOSRAVI *et al*. (2021) report, in their work, an experiment where the nanoparticle of 120 and 260 nm was pre-soaked for hours before the flush, resulting and better retention of SiN in porous space leading to the recovery of more oil.

The test done with silica nanoparticles with 100 nm had a favorable result and, accordingly to the PAK *et al.* (2018) research hypothesis, the nanoparticle action in

EOR could have a better performance by increasing the concentration because SiN action decreases IFT with the rise of these. So, a second phase of experiments was conducted to evaluate this.

## 4.2 SECOND PHASE EXPERIMENTS

### 4.2.1 Nanoparticle Characterization

Since the firsts flow experiments showed the efficiency of the silica nanoparticles of 100 nm, they were synthesized again for the following experiments.

TABLE 4.1 shows the conducted characterization nanoparticle analysis values. As observed above, the hydrodynamic diameter from the DLS measurement was ~100 nm, as desired, moreover, its PDI < 0.1 (polydispersity index) value indicated that the nanoparticles are monodisperse and their sizes are equal to or close to medium hydrodynamic diameter. The Polydispersity Index is a significant parameter since it implies the deviation of particles in the sample from their average diameter and is one of the main specifications of the Stöber synthesis route chosen.

TABLE 4.1 – Nanoparticle characteristics

| **Analyses** | **Values** |
|---|---|
| DLS | 101.1 nm |
| PDI | 0.04 |
| ZP | -(34,8) mV |
| Concentration | 0.3 wt% |

SOURCE: AUTHOR (2021).

The graph in FIGURE 4.7 demonstrates the size distribution of silica nanoparticles and their low polydispersity.

FIGURE 4.7 – Size distribution of silica nanoparticles determined from the DLS technique

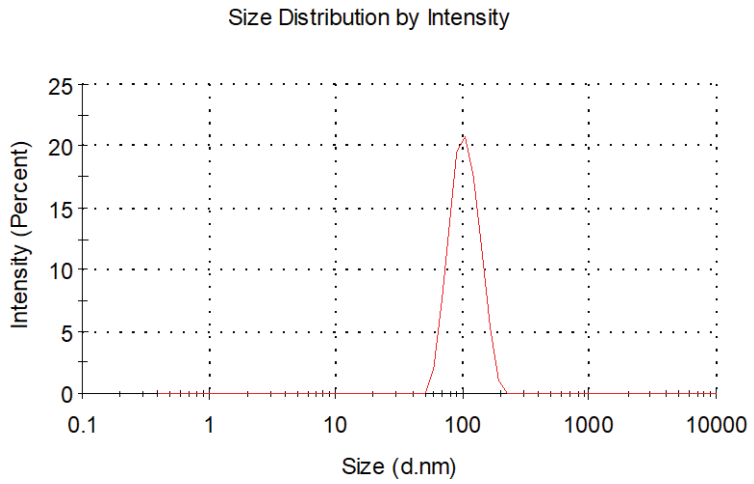


SOURCE: AUTHOR (2021).

Zeta potential measurement was also made, and this parameter demonstrates the relation between nanoparticle charge surface and its size (TABLE 4.1). The ZP negative value found is related to deprotonated silanol groups (-Si-O-) present in the nanoparticle surface, as expected (BHATTACHARJEE, 2016).

The image from SEM analysis was performed to complementation of DLS results. FIGURE 4.8 shows the sphere shape and low polydispersity of silica nanoparticles from Stöber route synthesis, making them appropriate for minimizing the size influence for enhanced oil recovery.

FIGURE 4.8 – SEM analysis of silica nanoparticle

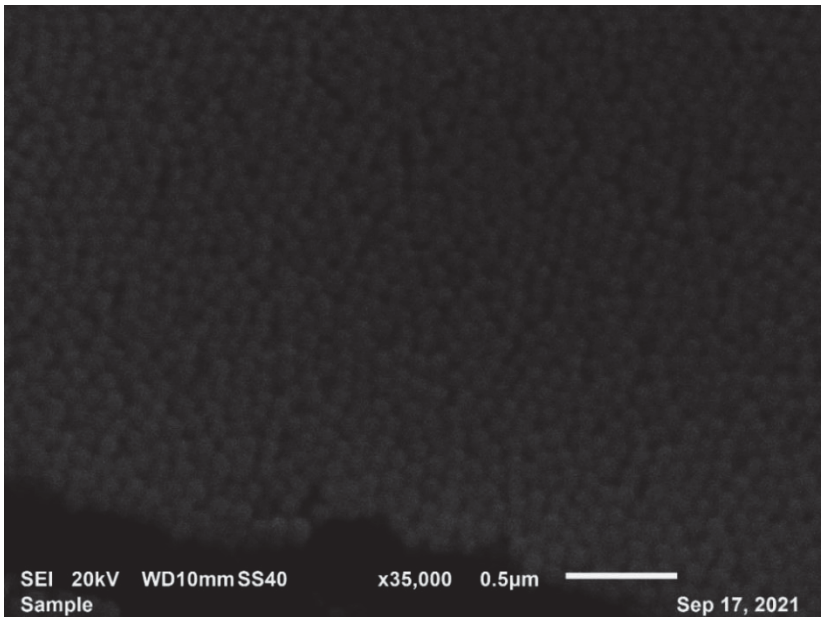


SOURCE: AUTHOR (2021).

### 4.2.2 EOR Nanoflooding

As previously mentioned, the second stage nanoflooding experiment was conducted using rock samples classified as more water-wet. Thereby as expected in the waterflooding flush, water had removed a significant percentage of the initial oil in place (FIGURE 4.9); as the rock surface has an adhesion preference for water molecules, the oil was easily displaced.

FIGURE 4.9 – Recovery efficiency in ooid core sample graph using NP of 100 nm at different concentrations (0.1, 0.2 and 0.3 wt%)

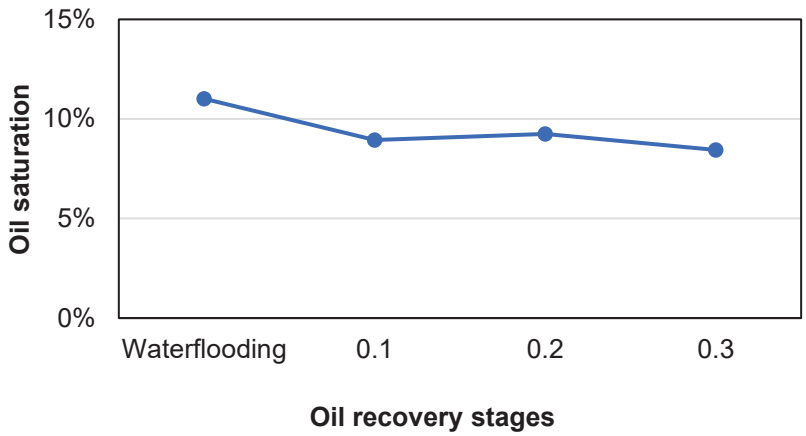


SOURCE: AUTHOR (2022).

Most rock samples have a mixed-wet porous medium because of the different mineral compositions in diverse porous, thus, generating local surfaces in the rock oil-wet (BUCKLEY, 1998), like the sample used in this experiment, leading to a remaining oil adhered to the ooid surface (FIGURE 4.10 [B]).

FIGURE 4.10 – 3D rendering of oil volumes in the recovery steps, using 100 nm silica nanoparticle in ooid core sample. (A) initial oil saturation, (B) waterflooding, nanoflooding (C) 0.1 wt%, (D) 0.2 wt% and (E) 0.3 wt%.

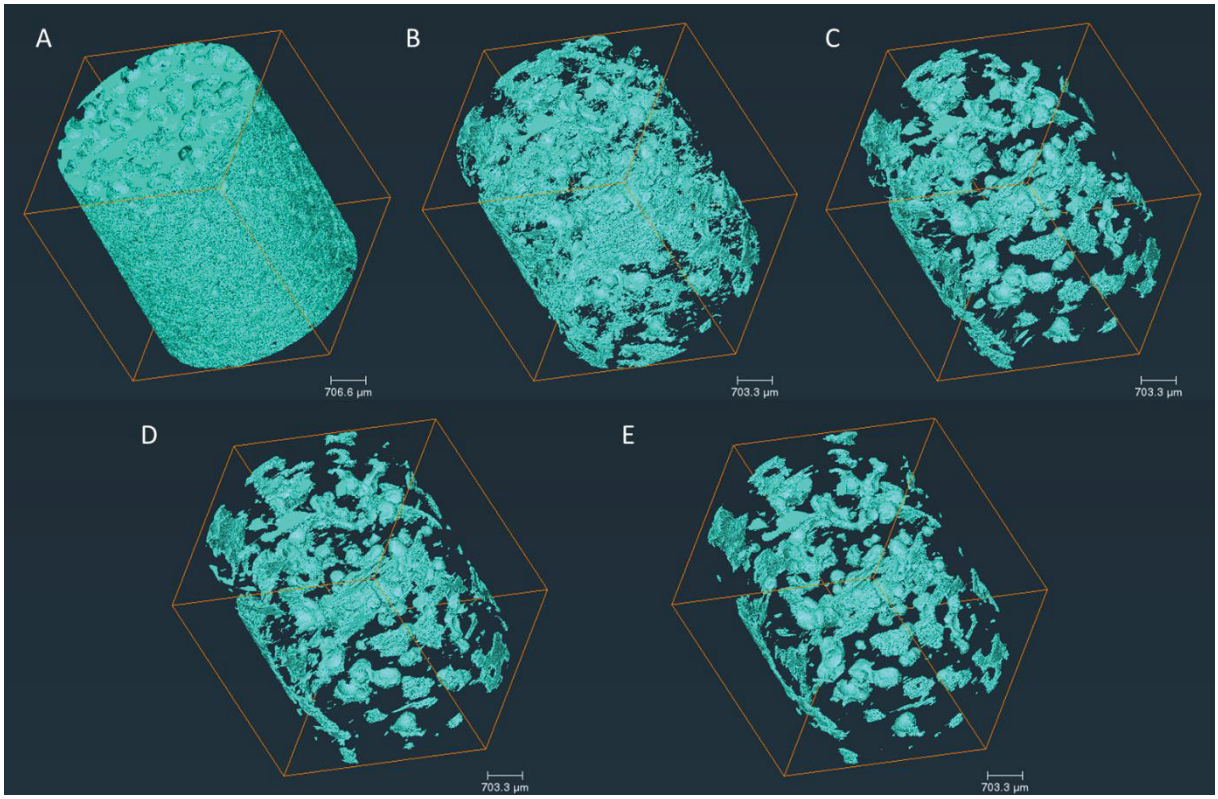


SOURCE: AUTHOR (2022).

In the EOR stage using the silica nanoparticles of 100 nm, as shown in FIGURE 4.9, the oil recovery achieved was lower compared to the first phase experiment. Only 2% of the remaining was recovered from the ooid porous sample, flushing SiN at 0.1 wt%. And for the following concentrations, 0.2 and 0.3 wt%, the result was a slight increase in oil percentage, subsequently, less than 1% of the oil was removed. This behavior was similar to the study performed with SiN-30 and 60 nm and in the work of PAK *et al*. (2018), which also used a rock sample water-wet.

Although the expected result was an increase in oil recovery by increasing the nanoparticle's concentration (ALVAREZ-BERRIOS *et al*., 2018), the nanoparticle's surface charge had a stability limitation because of silanol groups at the surface of nanoparticles, which allows it remains dispersed in the solution. YOUSSIF *et al*. (2018), in their work, reported better performance of SiN at 0.1 wt%, addressing the worse efficiency with higher concentration (0.5 wt%), to the aggregation of the nanoparticles, forming clusters, and blocking the flow pathway.

# 5 CONCLUSIONS

In this study, we used different X-ray sources for the microtomography technique as a characterization tool, which allowed us to analyze the nanoparticles' performance on recovery and remobilization of fluids inside mimic porous medium samples.

This technic permitted non-destructive imaging results of the oil dynamic inside the pore on a micro-scale.

In the first phase experiment, silica nanoparticles of 30 and 60 nm did not show a significant effect in recovering the remaining oil from waterflooding stage. Nonetheless, SiN-100 showed removal action, even at low concentrations (0.05 %wt), and it increased initial oil recovery to 78% in the last injection NP in 0.1 %wt.

Analyzing the core permeabilities and based on another study, we could consider that the silica nanoparticle's mechanisms of action are time-dependent. Further and different studies focusing on residence time could help to understand this process better.

The additional experiments of a second phase focused on studying the most efficient nanoparticle size, 100 nm, did not change the previous conclusion of the first phase experiment, where the lowest concentration employed in this work remains the optimal silica nanoparticle concentration, 0.05 wt%.

As for the use of a reservoir rock analog, the fact that it was a water-wet sample may influence the recovery investigation. In future projects, an aging process to change the permeability of the rock could improve this type of study, leading to a condition closer to reality.

Therefore, 100 nm diameter silica nanoparticles are still good candidates for application in enhanced oil recovery techniques. The silica nanoparticles showed efficiency in the recovery process, at low concentrations, possibly due to their nanometric scale and stability.

In addition, they are non-toxic nanoparticles and have a similar composition to natural orthosilicates, differently from other EOR methods.

## REFERENCES

AGÊNCIA NACIONAL DO PETRÓLEO GÁS NATURAL E BIOCOMBUSTÍVEIS (BRASIL). **Anuário estatístico brasileiro do petróleo, gás natural e biocombustíveis: 2020**. Rio de Janiero: [s.n.]. Disponível em: <www.anp.gov.br>.

ALI, J. A. *et al*. **Recent advances in application of nanotechnology in chemical enhanced oil recovery: Effects of nanoparticles on wettability alteration, interfacial tension reduction, and flooding**. Egyptian Journal of Petroleum. Egyptian Petroleum Research Institute,1 dez. 2018.

ALSOFI, A. M.; WANG, J.; KAIDAR, Z. F. SmartWater synergy with chemical EOR: Effects on polymer injectivity, retention and acceleration. **Journal of Petroleum Science and Engineering**, v. 166, jul. 2018.

ALVAREZ-BERRIOS, M. P. *et al*. Effect of the surface charge of silica nanoparticles on oil recovery: wettability alteration of sandstone cores and imbibition experiments. **International Nano Letters**, v. 8, n. 3, p. 181–188, 6 set. 2018.

AMERICAN ASSOCIATION OF PETROLEUM GEOLOGISTS. **A color guide to the petrography of carbonate rocks : grains, textures, porosity, diagenesis**. [s.l.] American Association of Petroleum Geologists, 2003.

ANDERSON, W. G. **Wettability Literature Survey - Part 6: The Effects of Wettability on Waterflooding**. [s.l: s.n.].

ARCHILHA, N. L. **Quantificação de parâmetros geométricos do sistema poroso por tomografia de raios X e análise da influência em propriedades físicas de rochas carbonáticas**. Macaé: [s.n.].

BHATTACHARJEE, S. **DLS and zeta potential - What they are and what they are not? Journal of Controlled Release.** Elsevier B.V., 10 ago. 2016.

BRITISH PETROLEUM. **BP Statistical Review of World Energy 2020**. [s.l: s.n.]. Disponível em: <www.bp.com/statisticalreview.>.

BUCKLEY, J. S. **Evaluation of reservoir wettability and its effects on oil recovery: Annual Report**. [s.l: s.n.].

CHANDLER, J. Stewardship of offshore petroleum: Where is the value? **Marine Policy**, v. 81, p. 64–70, 1 jul. 2017.

CHATZIS, I.; MORROW, N. R. Correlation of Capillary Number Relationships for Sandstone. **Society of Petroleum Engineers journal**, v. 24, n. 5, p. 555–562, 1984.

CNUDDE, V.; BOONE, M. N. High-resolution X-ray computed tomography in geosciences: A review of the current technology and applications. **Earth-Science Reviews**, v. 123, p. 1–17, ago. 2013.

COSTA, G. S. R.; VASCONCELOS, G. J. Q.; ARCHILHA, N. L. Fluid Injection System for X-ray Tomography Experiments. **Journal of Physics: Conference Series**, v. 2380, n. 1, p. 012110, 1 dez. 2022.

DING, F.; GAO, M. **Pore wettability for enhanced oil recovery, contaminant adsorption and oil/water separation: A reviewAdvances in Colloid and Interface Science.**Elsevier B.V., 1 mar. 2021.

ERKETIN, Turgay; ABOU-KASSEM, Jamal H.; KING, Gregory R. **Basic applied reservoir simulation.** Richardson: Society of Petroleum Engineers, 2001.

FOREIGN AND COMMONWEALTH OFFICE. **Oil and gas governance and efficiency study:** Output 1 report: Review of policy and regulatory frameworks for enhanced oil recovery (EOR) and improved oil recovery (IOR). [S.l.]: Amec Foster Wheeler Environment & Infrastructure Uk Limited, 2017. Disponível em: http://www.anp.gov.br/images/Palestras/Aumento_Fator_Recuperacao/Relatorio1_AMEC.pdf. Acesso em: 06 fev. 2019.

FORREST, F.; CRAIG, J. **The Reservoir Engineering Aspects of Waterflooding**. [s.l: s.n.].

FUSSEIS, F. *et al*. A brief guide to synchrotron radiation-based microtomography in (structural) geology and rock mechanics. **Journal of Structural Geology**, v. 65, p. 1–16, ago. 2014.

GAO, Y. *et al*. Pore-scale imaging with measurement of relative permeability and capillary pressure on the same reservoir sandstone sample under water-wet and mixed-wet conditions. **Advances in Water Resources**, v. 146, 1 dez. 2020.

GARNES, J. M. *et al*. **Capillary Number Relations for Some North, Sea Reservoir Sandstones**. All Days. **Anais**...SPE, 22 abr. 1990. Disponível em: <https://onepetro.org/SPEIOR/proceedings/90EOR/All-90EOR/Tulsa,%20Oklahoma/67722>

GHOUS, A. *et al*. **3D Characterisation of Microporosity in Carbonate Cores**. [s.l: s.n.].

GONZALES, Rafael C.; WOODS, Richard E. **Digital Image Processing**. New Jersey: Prentice-Hall, 2002.

GUO, H. *et al*. **A Novel Alkaline-Surfactant-Foam EOR Process**. All Days. **Anais**...SPE, 19 jul. 2011.

GUO, H. *et al*. **Review of capillary number in chemical enhanced oil recovery**. Society of Petroleum Engineers - SPE Kuwait Oil and Gas Show and Conference. **Anais**...Society of Petroleum Engineers, 2015.

HAN, M. *et al*. **Development of Chemical EOR Formulations for a High Temperature and High Salinity Carbonate Reservoir**. All Days. **Anais**...IPTC, 26 mar. 2013.

HANKE, R. *et al*. X-ray Microtomography for Materials Characterization. In: **Materials Characterization Using Nondestructive Evaluation (NDE) Methods**. [s.l.] Elsevier Inc., 2016. p. 45–79.

HENDRANINGRAT, L.; LI, S.; TORSÆTER, O. **Effect of some parameters influencing enhanced oil recovery process using Silica Nanoparticles: An experimental investigation**. Society of Petroleum Engineers - SPE Reservoir Characterisation and Simulation Conference and Exhibition, RCSC 2013: New Approaches in Characterisation andModelling of Complex Reservoirs. **Anais**...2013.

INTERNATIONAL ENERGY AGENCY. **Storing CO2 through Enhanced Oil Recovery: Combining EOR with CO2 storage (EOR+) for profit**. Paris: [s.n.]. Disponível em: <www.iea.org/t&c/>.

JIANG, R.; LI, K.; HORNE, R. **A Mechanism Study of Wettability and Interfacial Tension for EOR Using Silica Nanoparticles**. Day 3 Wed, October 11, 2017. **Anais**...SPE, 9 out. 2017. Disponível em: <https://onepetro.org/SPEATCE/proceedings/17ATCE/3-17ATCE/San%20Antonio,%20Texas,%20USA/193141>

KAK, A. C.; SLANEY, M. **Principles of Computerized Tomographic Imaging**. Nova York: IEEE, 327p., 1988.

KEYKHOSRAVI, A. *et al*. Comparative study of different enhanced oil recovery scenarios by silica nanoparticles: An approach to time-dependent wettability alteration in carbonates. **Journal of Molecular Liquids**, v. 324, p. 115093, fev. 2021.

KHAYATI, H. *et al*. An experimental investigation on the use of saponin as a non-ionic surfactant for chemical enhanced oil recovery (EOR) in sandstone and carbonate oil reservoirs: IFT, wettability alteration, and oil recovery. **Chemical Engineering Research and Design**, v. 160, ago. 2020.

LEE, M. H.; BEYER, F. L.; FURST, E. M. Synthesis of monodisperse fluorescent core-shell silica particles using a modified Stöber method for imaging individual particles in dense colloidal suspensions. **Journal of Colloid and Interface Science**, v. 288, n. 1, p. 114–123, 1 ago. 2005.

LEVITT, D. *et al*. **Identification and Evaluation of High-Performance EOR Surfactants**. All Days. **Anais**...SPE, 22 abr. 2006.

LI, S. *et al*. **Silica Nanoparticles Suspension for Enhanced Oil Recovery: Stability Behavior and Flow Visualization**. Day 4 Thu, June 14, 2018. **Anais**...SPE, 11 jun. 2018. Disponível em: <https://onepetro.org/SPEEURO/proceedings/18EURO/4-18EURO/Copenhagen,%20Denmark/216169>.

LI, S.; TORSÆTER, O. **The Impact of Nanoparticles Adsorption and Transport on Wettability Alteration of Intermediate Wet Berea Sandstone**. Day 3 Wed, January 28, 2015. **Anais**...SPE, 26 jan. 2015.

MIQUELES, E.; KOSHEV, N.; HELOU, E. S. A Backprojection Slice Theorem for Tomographic Reconstruction. **IEEE Transactions on Image Processing**, v. 27, n. 2, p. 894–906, 1 fev. 2018.

MOHSENATABAR FIROZJAII, A.; SAGHAFI, H. R. **Review on chemical enhanced oil recovery using polymer flooding: Fundamentals, experimental and numerical simulationPetroleum**KeAi Communications Co., , 1 jun. 2020.

NAFISIFAR, A.; KHAKSAR MANSHAD, A.; REZA SHADIZADEH, S. Evaluation of a new green synthesized surfactant from linseeds - chemical EOR implications from sandstone petroleum reservoirs. **Journal of Molecular Liquids**, v. 342, nov. 2021.

NEGIN, C.; ALI, S.; XIE, Q. **Application of nanotechnology for enhancing oil recovery – A reviewPetroleum**KeAi Communications Co., , 1 dez. 2016.

PAK, T. *et al*. The Dynamics of Nanoparticle-enhanced Fluid Displacement in Porous Media - A Pore-scale Study. **Scientific Reports**, v. 8, n. 1, 1 dez. 2018.

PAK, T.; ARCHILHA, N. L.; AL-IMARI, R. Application of nanotechnology in removal of NAPLs from contaminated aquifers: a source clean-up experimental study. **Clean Technologies and Environmental Policy**, v. 20, n. 2, p. 427–433, 13 mar. 2018.

PATEL, A. *et al*. **Evaluating Feasibility of Hydrophilic Silica Nanoparticles for In-Situ Emulsion Formation in Presence of Co-Surfactant: An Experimental Study**. Day 3 Wed, April 26, 2017. **Anais**...SPE, 24 abr. 2017. Disponível em: <https://onepetro.org/SPESATS/proceedings/17SATS/3-17SATS/Dammam,%20Saudi%20Arabia/196187>.

PETH, S. **Applications of microtomography in soils and sediments**. [s.l: s.n.]. v. 34.

RAMOS, G. A. R.; AKANJI, L. T.; AFZAL, W. A Novel Surfactant–Polymer/Alkaline–Surfactant–Polymer Formulation for Enhanced Oil Recovery (EOR) Processes. **Energy & Fuels**, v. 34, n. 2, 20 fev. 2020.

ROSA, Adalberto José; CARVALHO, Renato de Souza; XAVIER, José Augusto Daniel. **Engenharia de Reservatórios de Petróleo.** Rio de Janeiro: Interciência, 2006. 832 p.

ROSTAMI, P. *et al*. Enhanced oil recovery using silica nanoparticles in the presence of salts for wettability alteration. **Journal of Dispersion Science and Technology**, v. 41, n. 3, p. 402–413, 23 fev. 2020.

RÜCKER, M. *et al*. Relationship between wetting and capillary pressure in a crude oil/brine/rock system: From nano-scale to core-scale. **Journal of Colloid and Interface Science**, v. 562, p. 159–169, 7 mar. 2020.

SATTER, A.; IQBAL, G. M. Reservoir fluid properties. In: **Reservoir Engineering**. [s.l.] Elsevier, 2016. p. 81–105.

SHAKEEL, M. *et al*. Experimental analysis of oil displacement by hybrid engineered water / chemical EOR approach in carbonates. **Journal of Petroleum Science and Engineering**, v. 207, dez. 2021.

SHENG, James J. **Modern chemical enhanced oil recovery:** theory and practice. [S.l.]: Elsevier Inc., 2011.

SIRCAR, A. *et al*. **Applications of nanoparticles in enhanced oil recoveryPetroleum Research**KeAi Publishing Communications Ltd., , 2021.

SMALLEY, P. C. *et al*. Reservoir Technical Limits: A Framework for Maximizing Recovery From Oil Fields. **SPE Reservoir Evaluation & Engineering**, v. 12, n. 04, p. 610–629, 8 set. 2009.

SPEIGHT, J. Reservoirs and reservoir fluids. In: **Shale Oil and Gas Production Processes**. [s.l.] Elsevier, 2020. p. 139–220.

TERRA, G. J. S. *et al*. Classificação de rochas carbonáticas. **Boletim de Geociências Petrobrás**, v. 18, n. 1, p. 9–29, 2010.

THOMAS, José Eduardo (org.). **Fundamentos da Engenharia de Petróleo**. Rio de Janeiro: Interciência, 2001.

ULMISHEK, G. F.; KLEMME, H. D. **Depositional Controls, Distribution, and Effectiveness of World's Petroleu·m Source Rocks**. [s.l: s.n.].

VISHNYAKOV, V. *et al*. Chemical EOR. In: **Primer on Enhanced Oil Recovery**. [s.l.] Elsevier, 2020. p. 141–159.

WANG, D. et al. Mechanism Discussion of Nanofluid for Enhanced Oil Recovery: Adhesion Work Evaluation and Direct Force Measurements between Nanoparticles and Surfaces. **Energy and Fuels**, v. 32, n. 11, p. 11390–11397, 15 nov. 2018.

WANG, W.; LIU, Y.; GU, Y. Application of a Novel Polymer System in Chemical Enhanced Oil Recovery (EOR). **Colloid & Polymer Science**, v. 281, n. 11, 1 out. 2003.

WANG, Y. *et al*. Pore-scale experimental study on EOR mechanisms of combining thermal and chemical flooding in heavy oil reservoirs. **Journal of Petroleum Science and Engineering**, v. 185, fev. 2020.

WILLMOTT, P. R. **An introduction to synchrotron radiation:** techniques and applications. [S.l.]: John Wiley & Sons, 2011.

WYATT, K.; PITTS, M. J.; SURKALO, H. **Economics of Field Proven Chemical Flooding Technologies**. All Days. **Anais**...SPE, 20 abr. 2008. Disponível em: <https://onepetro.org/SPEIOR/proceedings/08IOR/All-08IOR/Tulsa,%20Oklahoma,%20USA/143947>.

YOUSSIF, M. I. *et al*. Silica nanofluid flooding for enhanced oil recovery in sandstone rocks. **Egyptian Journal of Petroleum**, v. 27, n. 1, p. 105–110, mar. 2018.

ZHANG, Z.; LI, J.; ZHOU, J. Microscopic Roles of “Viscoelasticity” in HPMA polymer flooding for EOR. **Transport in Porous Media**, v. 86, n. 1, 15 jan. 2011.